# Toward a Consensus Historical AVHRR Reflectance Calibration

**Personnel:**

Andrew Heidinger, Christine Molling, William Straka

**Funded by:**

NA07OAR4310199

**Project Description**

The Advanced Very High Resolution Radiometer (AVHRR) flying on NOAA and EUMETSAT polar orbiters has a long data record (1979-present); and with its global, daily coverage and moderately high resolution (1-4km) it can resolve many cloud and surface features. Unfortunately, sensor degradation and lack of on-board calibration for channels 1 (red) and 2 (NIR) require post-launch calibration efforts in order for these data to be useful for detecting long term climate change.

Although calibration research has been conducted since the early days of the instrument, there is still quite a bit of disagreement among the various published calibrations – on the order of 10%. This goal of this project is to study past calibration efforts, bring together current AVHRR calibration researchers, and design a set of guidelines for calibration that will bring differing methodologies within a 3-4% consensus. In addition, another goal of this project to generate a new version of the AVHRR Pathfinder Extended Data-set that benefits from the improved calibration knowledge.

**Progress for Year 2: June 2009 – June 2010**

During the second year of this effort, two manuscripts were submitted and accepted for publication in the International Journal of Remote Sensing. The first was led by Christine Molling and documented the current state of the AVHRR reflectance calibration. The second was led by Andrew Heidinger and describes the new and improved AVHRR reflectance calibration done under this project. It is important to note that this new calibration is the first to be generated in a consistent manner for all AVHRRs that have ever flown. For reference, Figure 1 illustrates the main points of the PATMOS-x reflectance calibration developed here.

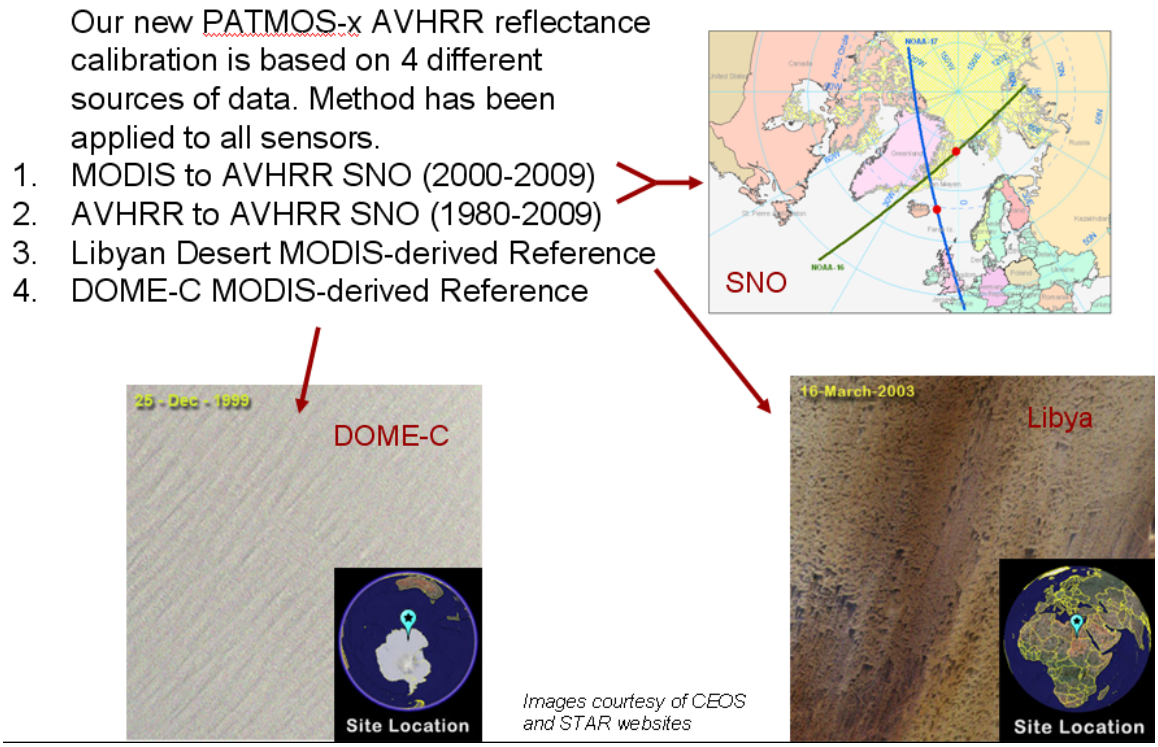


**Figure 1 Schematic Illustration of our new technique for calibration. The PATMOS-x calibration applies the 4 main techniques developed at NESDIS to the entire AVHRR record. By using these disparate techniques, we gain robustness over the entire dynamic range.**

Figure 2 shows an example of a comparison of the existing calibration information to that derived in this project. This figure shows a time-series of the clear-sky Greenland reflectance. This time period includes the transition from one AVHRR to another (NOAA-12 to NOAA-15). Given the stability of the Greenland Ice Sheet, this time series should be stable. However, the prelaunch and ISCCP time-series show an artifact at the satellite transition time. The new calibration (PATMOS-x) generates a smoother time-series that we argue is more accurate and suitable for climate applications.

We have also spent the second year validating our calibration and the product time-series that rely on it. Figure 3 shows a time-series of cloud optical depth generated via PATMOS-x using the new calibration. The region is a region dominated by marine stratus which should produce a relatively constant set of cloud properties. The adjusted line is a diurnally corrected time series and involves no satellite to satellite adjustment. The red vertical lines indicate the transitions from one AVHRR to another. The important point of this figure is that there is no apparent artifact in this time-series which increases our confidence in the calibration accuracy and stability.

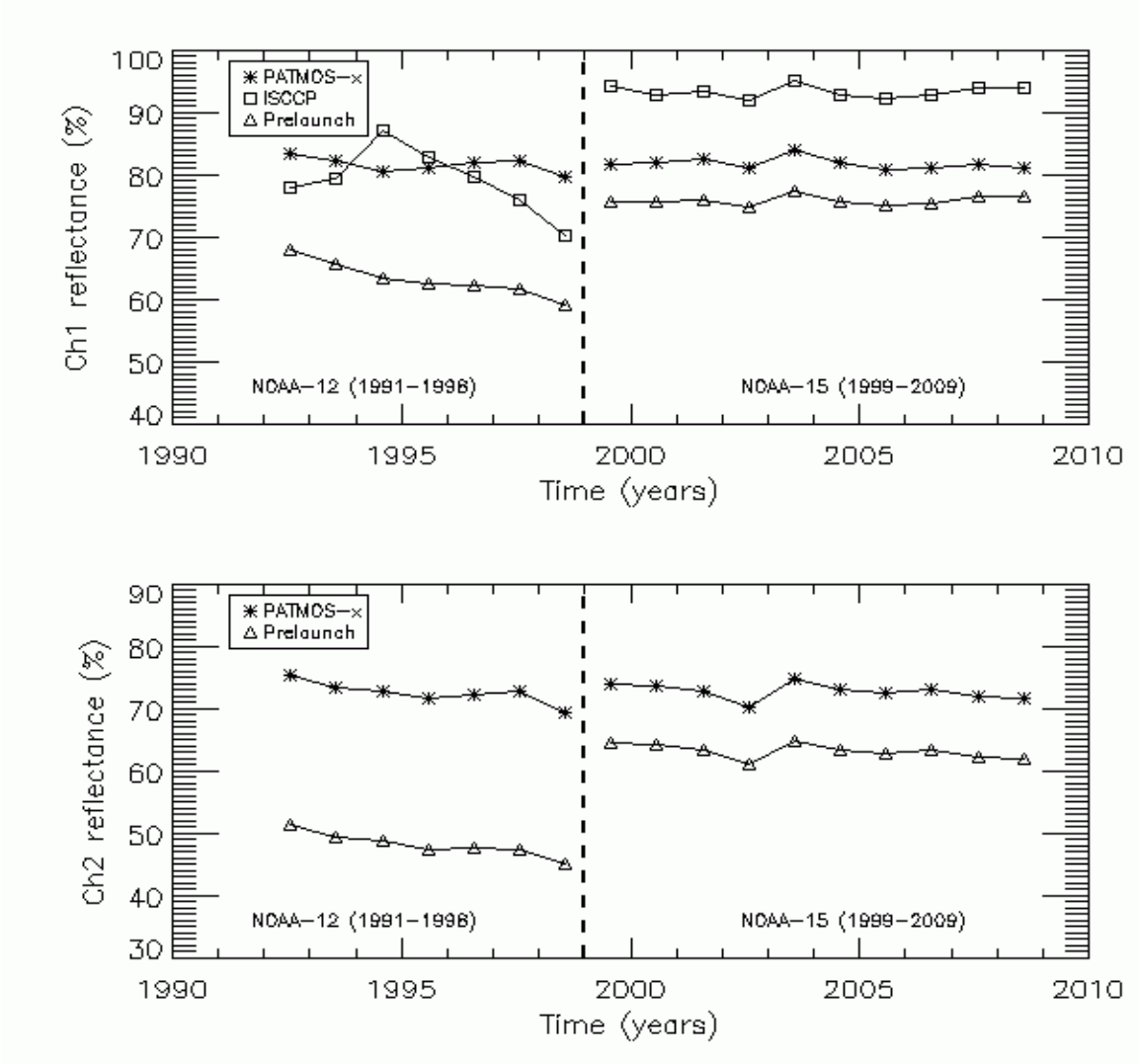


**Figure 2 Time-series of Greenland reflectance during the NOAA-12 to NOAA-15 transition. Data are computed using the ISCCP, PATMOS-x and Prelaunch calibrations.**

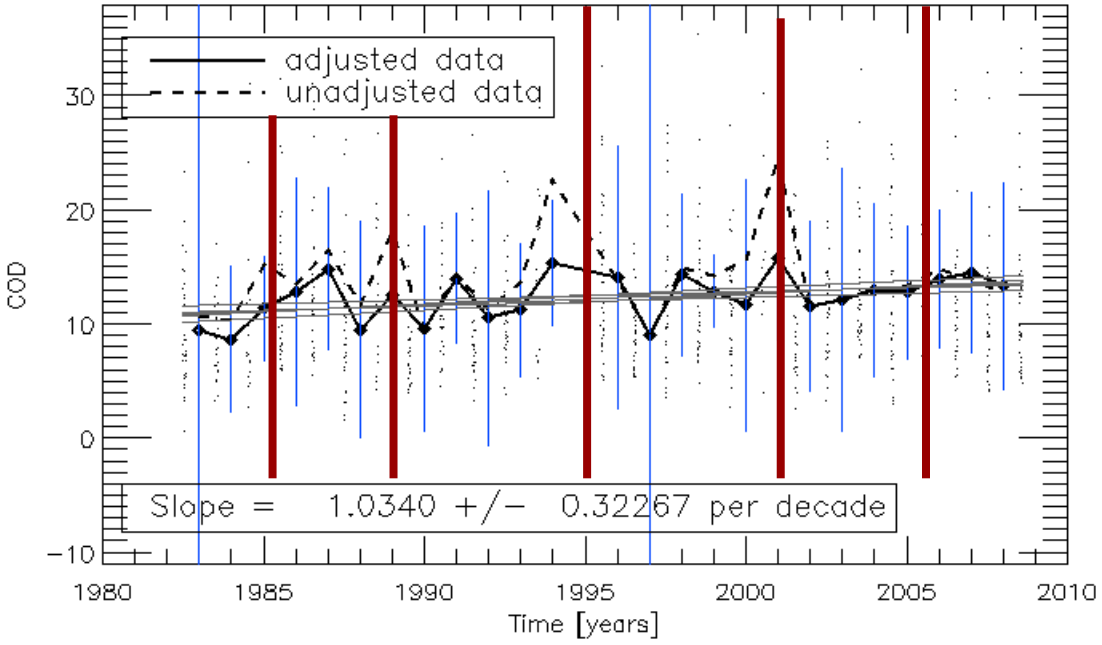


**Figure 3 Time-series of cloud optical depth (COD) from the AVHRR in the North-Eastern Pacific off the Coast of California. The vertical lines indicate the periods of transition from one satellite to another. COD time series are shown since they are highly dependent on the reflectance calibration. The adjusted line represents a simple diurnal correction and represents no normalization of the results. The lack of artifacts at the transitions between satellite and the overall stability increase our confidence in our calibration.**

### *Collaborations*

Throughout this year, we have been collaborating with colleagues in the community who are reliant on the information we are deriving. To date, the following groups have asked for and been given our calibration results.

1. The International Cloud Climatology Satellite Project (ISCCP)
2. The EUMETSAT Climate Monitoring Satellite Application Facility (CM-SAF)
3. Professor's Stefan Wunderle's group at the University of Bern, Switzerland.

In addition, this calibration information is being submitted for approval as Global Space Based Intercalibration Committee (GSICS) data-set. Also, we intend to brief the community on these results at the CalCon Conference in August 2010.

### *Future Work*

We are greatly appreciative of the support on this project. This effort has put us in a good position to expand this work. For example, we intend to apply these techniques to the 1.6 micron channel that is available on some recent AVHRRs. Also, we intend to include the analysis of deep convective cloud to validate the spectral consistency of these results.

## Publications/Conference Presentations

Molling, C., Heidinger, A., Straka III, W., and Wu, X., 2009: Calibrations for AVHRR channels 1 and 2: review and path toward consensus. (In press to IJRS)

Heidinger, A., Straka III, W., Molling, C., Pavolonis, M., Sullivan, J, 2009: and Deriving an Inter-sensor Consistent Calibration for the AVHRR Solar Reflectance Data Record. (in press to IJRS)

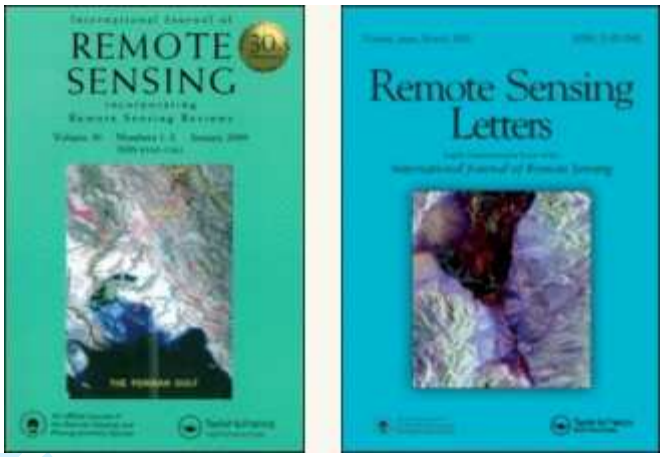


# Calibrations for AVHRR channels 1 and 2: review and path toward consensus

| | |
|---|---|
| Journal: | *International Journal of Remote Sensing* |
| Manuscript ID: | TRES-PAP-2009-0732.R1 |
| Manuscript Type: | IJRS Research Paper |
| Date Submitted by the Author: | 13-May-2010 |
| Complete List of Authors: | Molling, Christine; UW Madison, CIMSS/SSEC<br>Heidinger, Andrew; NOAA/NESDIS, Office of Research and Applications<br>Straka III, William; University of Wisconsin, CIMSS<br>Wu, Xiangqian; NOAA/NESDIS, STAR |
| Keywords: | AVHRR, CALIBRATION, CLIMATOLOGY |
| Keywords (user defined): | |

# Calibrations for AVHRR channels 1 and 2: review and path toward consensus

CHRISTINE C. MOLLING*†, ANDREW K. HEIDINGER‡, WILLIAM C. STRAKA III† and XIANGQIAN WU§

†Cooperative Institute for Meteorological Satellite Studies, University of Wisconsin, 1225 West Dayton Street, Madison, WI 53705, USA

‡NOAA/NESDIS Center for Satellite Applications and Research, 1225 West Dayton Street, Madison, WI 53705, USA

§NOAA/NESDIS Center for Satellite Applications and Research, 5200 Auth Road, Camp Springs, MD 20746-4304, USA

Short title for running headlines:

**Consensus for AVHRR channels 1 & 2**



* Corresponding author. Email: cmolling@wisc.edu, TEL: 608-265-5350, FAX: 608-262-5974

**Calibrations for AVHRR channels 1 and 2: review and path toward consensus**

(*Received dd Month 2009; in final form dd Month 2010*)

Formatted: Highlight
Formatted: Highlight
Deleted: 20xx
Deleted: earth

The over three decade long data record from the Advanced Very High Resolution Radiometer (AVHRR) is ideal for studies of Earth's changing climate. However, the lack of on-board calibration requires that the solar channels be recalibrated after launch. Numerous calibration studies have been conducted, but significant differences remain among the calibrations. This study is one effort to outline a path toward consensus calibration of the AVHRR solar channels. The characteristics of the polar orbiting satellites bearing the AVHRRs, the AVHRR instruments and data are described as they are related to calibration. A review of past and current calibration studies is also presented and examples of their lack of consensus shown. A list of Consensus Items is then provided, that if followed by the AVHRR calibration community, should bring the various calibration methods to within the small percent difference required for long term climate detection.

## 1. Introduction

As one of the instruments on the National Oceanographic and Atmospheric Administration's (NOAA's) Polar-orbiting Operational Environmental Satellite (POES) series, the Advanced Very High Resolution Radiometer (AVHRR) has a greater than three decade long record of high resolution data, ideally suitable for climate studies. Beginning in 1978 with the launch of TIROS-N and continuing through the current time with NOAA-19 and Metop-A of the European Organisation for the Exploitation of Meteorological Satellites, the imagery in the visible, near infrared and thermal infrared spectral regions can provide insight globally into changes in clouds, vegetation cover, aerosols and sea surface temperature over the past 30 years. One barrier to the use of these data for climate studies is the lack of on-board calibration for AVHRR channels in the visible (channel 1) and near infrared (channel 2). Because of the wide differences in post-launch calibrations, NOAA's Climate Program Office has funded a project whose purpose is to map out a path that can lead the calibration community toward consensus calibrations for AVHRR channels 1 and 2. This paper is part of that effort. In this paper, we present a description of the AVHRR instrument, data and issues related to the challenge of calibrating channels 1 and 2. We review the published body of calibration efforts, identifying those still active. We then present several components of calibration methodology, which if followed by the scientific community, will lead to a consensus set of calibrations for AVHRR channels 1 and 2, suitable for long term climate studies.

## 2. The AVHRR

This section summarizes facts related to the satellites bearing the AVHRR, the AVHRR instruments themselves and the data available from the AVHRR. The descriptions of the satellites, AVHRR instruments and data versions found here are taken from the NOAA Polar Orbiter Data User's Guide (POD Guide, Kidwell 1998) and the NOAA KLM User's Guide with NOAA-N, -N' Supplement (KLM Guide, Robel 2009), unless

otherwise noted. A more detailed summary of the technical aspects of the AVHRR and applications of AVHRR data can be found in Cracknell (1997).

### 2.1 The Satellites

The Advanced Very High Resolution Radiometer's history of service began in 1978 with the launch of TIROS-N and continues through today. Table 1 shows the launch and service dates of the operational POES spacecraft and the times of their ascending and descending nodes at launch. Failed satellites in the POES series were NOAA-B, launched 29 May 1980, which failed to achieve orbit and NOAA-13, launched 9 August 1993, which failed due to a short circuit in the solar array. POES orbits were positioned to provide "morning" and "afternoon" views. The several "morning" satellites that cross at approximately 7:30 and 19:30 local time frequently view scenes that are not sunlit, or are near the day/night terminator on both the ascending and descending halves of each orbit. The "afternoon" satellites view one day and one night swath per orbit. All NOAA POES through NOAA-15 had orbits that drifted over time, so that for any one location on the Earth, the local time of overpass and the instrument's view angle changed after launch. Orbit stabilization was available NOAA-16 and after.

Deleted: earth

### 2.2 The AVHRR Instrument

The AVHRR was built in several versions. Table 2 provides a summary of the characteristics of the four versions. On all AVHRR models, channel 1 and channel 2 are "solar" channels, that is, they sense regions of the electromagnetic spectrum where the measured energy originates from the sun and is reflected toward the instrument. These two channels are calibrated before the instrument is launched, but neither of the solar channels have on-board calibration. The thermal channels (channels 3 through 5 when available) have on-board calibration. The AVHRR/3 has a channel 3a, which senses a region of the spectrum that contains both solar reflected energy and Earth emitted energy. The AVHRR spectral range for channel 1 differs substantially from the channel 1 range on the other AVHRR versions. The channel 2 spectral response is similar. The first two channels on NOAA-6 through Metop-A have spectral ranges similar on each of the platforms, although the spectral response functions vary somewhat from instrument to instrument. The pre-launch spectral response functions for the solar spectrum at the top of the atmosphere can be found in Kidwell (1998) and Robel (2009) which use the Neckel and Labs (1984) spectrum subsampled by Rossow et al. (1985). There appear to be some errors in these published response functions, however (Wu 2009). Plots using the corrected response functions (Wu 2009) and a more recent solar spectrum (Thuillier et al. 2003) can be found at Heidinger and Straka (2009).

Deleted: On TIROS-N, which had a total of four channels, the spectral ranges for channels 1 and 2 were 0.55-0.90 $\mu$ m and 0.725-1.10 $\mu$ m, respectively. The AVHRR/1 on NOAA-6, -8 and -10, also had four channels with somewhat different spectral ranges for some of the channels. The AVHRR/2 on NOAA-7, -9, -11, -12 and -14 had five channels and the AVHRR/3 on NOAA-15, -16, -17, -18, -19 and Metop-A have six.

Deleted: earth

Deleted: (channel 1 is approximately 0.58-0.68 $\mu$ m and channel 2 is approximately 0.725-1.10 $\mu$ m)

The first two channels of the AVHRR sense regions of the solar spectrum where the Earth's atmosphere absorbs energy for certain wavelengths. The channel 1 spectrum contains relatively weak atmospheric absorption bands for ozone and oxygen, but is fairly clear in terms of water vapour absorption. Channel 2 contains moderate atmospheric oxygen and strong water vapour absorption regions.

Deleted: earth

Incoming energy sensed by the AVHRR is converted to "counts" by way of a calibrated instrument gain for each channel. The earlier AVHRR instruments used a

single gain response for channels 1 and 2; that is the response of the instrument in terms of count was linear with incoming radiation in the band's spectral region. The AVHRR/3s on NOAA-15 and after have a dual gain response. Signal power below a cutoff level (approximately 25% reflectance, as calculated with the pre-launch calibration) has a higher gain (lower slope) in order to provide more brightness resolution in darker scenes, and power above the cutoff has a lower gain (higher slope). It is important to note that the term "gain" is sometimes misused. Some authors refer to the region of a dual gain AVHRR where the counts are below the cutoff and the reflectance:count slope is low as the "low gain" region. Gain is actually the inverse of slope, so that authors should refer to this as the "high gain" or "low slope" region and the region above the cutoff as the "low gain" or "high slope" region.

The AVHRR's instantaneous field of view (IFOV) is about 1.4 milliradians, or a circle approximately 1.1 km in diameter on the Earth's surface when the instrument is pointed at nadir. The scan angle maximum is ±55.4 degrees from nadir. At 55 degrees from nadir, the surface footprint is an oval approximately 6.5 km x 2.3 km. During each scan the AVHRR is also pointed into space to provide a diagnostic known as the "dark count" or "space count". This value, which is the instrument response for zero energy in the sensing band, is subtracted from the scene count before applying the calibration equation to compute reflectance or radiance. Occasionally, the moon is seen instead of deep space during the space view. Not all calibrations require subtracting the dark count.

Deleted: earth

### 2.3 The AVHRR Data

Data from the AVHRR are available in four types: APT – Automatic Picture Transmission direct readout, HRPT - High Resolution Picture Transmission direct readout, LAC – Local Area Coverage recorded HRPT and GAC – Global Area Coverage reduced resolution recorded AVHRR. HRPT and LAC are full-resolution data, but are limited in their coverage of the globe due to the few receiving stations (HRPT) and the limited data storage on the satellite (LAC). APT is a separate analogue VHF transmission (simple receiving equipment needed) of only two channels of the AVHRR selected by NOAA Spacecraft Operations Control – one visible and on IR channel during the day and two IR channels at night. APT is subsampled and linearized to produce 4km resolution data using the 8 most significant of the 10 bits and is continuously transmitted, but not recorded. GAC contains subsampled (every third scan) and averaged (4 adjacent samples with the 5$^{th}$ skipped) data, but is recorded and therefore global in coverage. GAC resolution is nominally 1.1 km x 4 km with a 3 km gap along the direction of orbit, but is generally considered to have 4 km resolution. Level 1b of HRPT, LAC and GAC are digital, raw data which are quality controlled and have navigation information appended. See Kidwell (1998) and Robel (2009) for more details on data types and formats.

### 2.4 Barriers to Calibration

Although the AVHRR instruments go through a calibration process before launch, vibration, vapour deposition, outgassing and other factors lead to a change in the instrument's response immediately after launch (Rao and Chen 1995). A new calibration

of AVHRR is required as soon as the instrument becomes operational. Sensors also degrade over time in the harsh space environment, causing the calibration to change during the satellite's term of service. Calibration of channels 1 and 2 of the AVHRR is made challenging due to issues related to the both the satellites and the instruments themselves. These issues are listed below.

The satellites in the "morning" and "afternoon" orbits see Earth targets in very different illumination. Certain Earth targets, such as White Sands, NM, are assumed to be Lambertian reflectors over a range of illumination angles (Smith et al. 1988). At large solar zenith angles and view angles, this assumption breaks down. Also, shadowing by clouds or surface features can contaminate the view excessively at large solar zenith angles (Loeb 1997, Masonis and Warren 2001). Thus the morning satellites are difficult to calibrate, and transferring a calibration between afternoon and morning satellites is not a simple task using ground targets. Orbit drift of pre-NOAA-16 satellites adds to the challenge, as calibration targets on Earth's surface are not viewed at the same solar zenith angles or satellite angles over time.

Deleted: earth

Deleted: earth

Channel 2 of the AVHRR contains a region of the spectrum having strong water vapour absorption by the atmosphere (as does channel 1 for TIROS-N). Because the amount of water vapour in the atmosphere varies greatly over time and from place to place, correcting for water vapour absorption is an important step in calibrating channel 2. Channel 1 contains a relatively weak ozone absorption band. Atmospheric ozone does vary temporally and spatially, but ozone variability is sometimes ignored in calibrating channel 1 (Vermote and Kaufman 1995, Loeb 1997). Both channels are impacted by atmospheric aerosols such as dust, pollution and volcanic ejecta, which also vary temporally and spatially. For example, the eruption of Mt. Pinatubo in 1991 created a global, long-lasting aerosol impact – the calibration of NOAA-11 in particular is made difficult from this eruption. Correcting for aerosol effects is a necessary step in calibrating channels 1 and 2, requiring additional data sources.

AVHRR data are georeferenced with navigation formulae that use a time stamp and spacecraft attitude angles. The satellite clocks drift, so a clock drift file is available to correct the data. Unfortunately, even with clock drift correction, pixel locations provided in the Level 1b data still contain errors from 2 to 10 km (Heidinger et al. 2002, Latifovic et al. 2005).

The switch from single gain AVHRR instruments to dual gain with NOAA-15 creates an additional calibration challenge. Instead of the need to fit only one slope and one intercept per channel to relate count to reflectance, two slopes and two intercepts are required. The two slopes require multiple calibration targets: at least one that produces reflectances over the 0% to 25% reflectance range and one other that produces reflectances over the 25% to 100% range. And as most calibration is done with GAC, those data which consist of pixel counts averaged from the two sides of the cutoff are a mixed average which cannot be deconvolved. This generates a cloud of points around the gain switch, resulting in more uncertainty in the high and low gain calibrations.

## 3. Review of Calibrations

In this section we provide a review of many of the AVHRR calibration studies, both past and current. The list of calibrations is not exhaustive, but does cover a wide variety.

### 3.1 Past Calibration Efforts

The need for post-launch calibration for channels 1 and 2 of the AVHRR was recognized quite early in the life of the series (Smith et al. 1988, Staylor 1990). Early calibration studies were based on a variety of methods. An initial absolute calibration for the AVHRR on NOAA-7 was done for White Sands, New Mexico by way of surface reflectance data and a radiative transfer model (Frouin and Gautier 1987). Later, the AVHRR on NOAA-9 was calibrated with high altitude aircraft measurements over White Sands, New Mexico (Smith et al. 1988). Aircraft measurements were also available for the calibration of NOAA-11, but questions remained about the aircraft calibrations of NOAA-11 and the instrument itself (Brest et al. 1997). The absolute calibration for NOAA-9 was seen as the most reliable, and subsequently was used to derive benchmark reflectances for several radiometrically stable Earth targets: Libyan Desert sites (Rao and Chen 1995), snow and ice fields in Greenland and Antarctica (Loeb 1997) and a collection of regions over the entire globe (Brest and Rossow 1992). Then, time dependent calibrations for the AVHRR on NOAA-9 were calculated. Radiances values of the stable ground targets established with calibrated NOAA-9 were subsequently used to calibrate AVHRRs on other satellites (Rao and Chen 1995 and 1996, Loeb 1997, Brest et al. 1997, Tahnk and Coakley 2001a, 2001b and 2002). A good review of the early calibration efforts for AVHRRS on NOAA-7, -9 and -11 can be found in Che and Price (1992).

Deleted: earth

In addition to the NOAA-9 aircraft-based series of calibration efforts, absolute calibrations independent of flight data were done for NOAA-7, -9 and -11 using atmospheric scattering, ocean glint and desert reflection (Kaufman and Holben 1993) and ocean and cloud views (Vermote and Kaufman 1995, Vermote and El Saleous 1996). Latifovic et al. (2005) used the Kaufman and Holben (1993) desert method in a piecewise linear fashion (Cihlar and Teillet 1995) to calibrate channels 1 and 2 of NOAA-7, -8, -9, -11, -12 and -14.

A few studies derived degradation rates but not an absolute calibration. Staylor (1990) calculated the degradation of channel 1 on NOAA-6, -7 and -9 via a bidirectional reflectance model. Bidirectional reflectance distribution functions for snow-covered targets in Antarctica and Greenland were used by Masonis and Warren (2001) to calculate the gain drift for channel 1 on NOAA-9, -10 and -11.

Several studies used other satellites with on-board calibration in order to cross-calibrate AVHRR: VIRS was used by Doelling et al. (2001) to calibrate NOAA-9 through NOAA-15, while a combination of VIRS and GOES-8 was used to calibrate NOAA-14 (Nguyen et al. 2004). Meteosat-8 was used to calibrate NOAA-17 (Doelling et al. 2007). MODIS was used in several studies. Heidinger et al. (2002) calibrated NOAA-16 directly from MODIS data. Doelling et al. (2004) used a deep convective cloud technique along with MODIS to provide absolute calibrations for channels 1 and 2 of NOAA-16 and -17. Vermote and El Saleous (2006) used MODIS and a radiative transfer model over a desert site to calibrate NOAA-16.

The majority of the calibration studies were done with GAC, subsampled GAC, or area averages of GAC. Only a few used HRPT or LAC (Smith et al. 1988, Heidinger et al. 2002, Cihlar et al. 2004, Latifovic et al. 2005). APT is used operationally (e.g.,

Heinzmann 1993) but is not generally used for calibration purposes, as the lower precision analogue signal, non-global coverage, and lack of a second visible channel make it less desirable for calibration than GAC, HRPT or LAC.

### 3.2 Current Calibration Efforts

Active calibration efforts for AVHRR are underway in several research groups. The NOAA/NESDIS Product Systems Branch releases calibrations on approximately a monthly basis for the operational satellites. These are found online at http://www.osdpd.noaa.gov/ml/ppp/notices.html. These are meant to be used for near-real-time data products. The NESDIS Center for Satellite Applications and Research (STAR) is also working on an improved calibration methodology with channel 1 on the afternoon satellites using a Libyan Desert target with the technique outlined in Wu (2004). The ISCCP group continues to calibrate channel 1 AVHRR according to their multiple target methodology described in Brest et al. (1997). The latest ISCCP calibrations for channel 1 are valid through 2006 and can be found on their web site http://isccp.giss.nasa.gov/. The group at the Canada Center for Remote Sensing (CCRS) presently uses piecewise linear interpolation for the NOAA post-launch calibration coefficients as described in Cihlar and Teillet (1995) and Latifovic et al. (2005). They plan to update their calibrations based on Tropical Deep Convective Cloud calibration method and recommendations from the NOAA-led activity toward community consensus calibration. The Land Long Term Data Record REASoN project is using the approach developed by Vermote and Kaufman (1995) to calibrate the afternoon AVHRRs. This approach calibrates channel 1 using clear ocean views and Rayleigh scattering. Then the channel 2:1 ratio is derived using high cloud reflectance. The channel ratio is used to transfer the calibration of channel 1 to 2. The latest results can be viewed at http://ltdr.nascom.nasa.gov/ltdr/ltdr.html. The CLAVR-x group continues its improvement of the PATMOS-x system (Heidinger and Straka 2009, Heidinger et al. 2010), including calibrating back as far as TIROS-N. The NASA Langley Research Center group also continues to expand and improve their AVHRR calibrations with the Deep Convective Cloud method (Doelling et al., 2004).

Deleted: PSB

Deleted: PPP/notices

Deleted: avhrr_calib_1

Deleted: 2009

### 3.3 Drawbacks in Calibration Efforts

Each of the past and current calibration techniques has its strengths and weaknesses. In this section we present a grab-bag of issues present in the various AVHRR calibration studies that may decrease the utility, accuracy and/or precision of any calibration, along with notes on methods to address the weaknesses.

Calibrations that cover both channels of all satellites are of greatest utility to AVHRR data users. Groups that calibrate only channel 1 (Brest et al. 1997, Masonis and Warren 2001) discourage their calibration from being used for products such as NDVI, which requires a calibrated channel 2. Groups that calibrate only the afternoon satellites neglect nearly half of the AVHRR record (Rao and Chen 1995, Rao and Chen 1996, Kaufman and Holben 1993, Vermote and El Saleous 1996). Calibration work on channel 2 and the more difficult morning satellites is to be strongly encouraged.

Calibrations that provide a degradation value, but no offset value are less useful, since more analysis must be done or other sources used to provide the offset (Masonis and Warren 2001). Calibrations that are a function of time derived over the entire length of the satellite's life and not just for a single point time are most useful. Studies that do not use the entire length of record for a particular satellite can derive trends unrepresentative of the entire life of the satellite (e.g., that for NOAA-11 in Masonis and Warren 2001). Calibrations that assume a constant linear degradation, an exponential degradation or some other form over the life of the satellite may not be representative of every AVHRR, so some flexibility in the form of the degradation equation is helpful. The piecewise-linear approach used in Cihlar and Teillet (1995) and Latifovic et al. (2005) is an example of a more flexible method.

Calibrations that assume a constant reflectance of an individual target dismiss the possibility that the target reflectance may indeed change over a long time – this is thought to be an issue more with desert than ice and snow covered targets (Masonis and Warren 2001), however with global warming, this may become an issue with ice fields as well. Independent evidence that a target does not change its reflectance would greatly increase confidence in any calibrations derived there. Independent reflectance measurements would also enable the detection of long term trends. The authors of the ISCCP calibration admit that their assumption that the global mean reflectance is constant in the long term allows for the detection of short term reflectance changes, but removes the possibility of detecting global reflectance trends longer than about 4 years (Brest et al. 1997). Calibrations based on a single target will be less statistically robust. Calibrations based on one type of target (e.g. ice fields) may not capture enough of the range in reflectance to calibrate both high and low gains on the AVHRR/3 instruments (Tahnk and Coakley 2002). Calibrations based only on polar targets will suffer from winter darkness (reduces number of possible data points over a year), large solar zenith angles (non-lambertian, low reflectance) and shadowing more than those at lower latitudes. A more robust method would be to use multiple targets with different reflectances in various latitudes, as done in Brest and Rossow (1992) and Brest et al. (1997).

Many calibrations are done in terms of reflectance, but assume the solar input is constant and only modified by the sun-Earth distance. Solar input is known to change by as much as 0.2% over a few days, depending on sunspot activity, and has shown an increase in total solar irradiance of 0.05% per decade from 1978 through 2002 (Willson and Mordvinov 2003). Although this is a small amount, this level of variation should be factored into any calibrations that do not use a solar input measurement. When calibrations are done in terms of radiance, they need to take into account changes in solar input, use a high quality solar spectrum and use corrected values for instrument response functions (Wu 2009). Assuming that an instrument's spectral response function is constant during degradation may not be correct – Vermote and Kaufman (1995) concluded that AVHRR channel 1 on both NOAA-9 and NOAA-11 experienced a shift in effective wavelength toward the red.

Deleted: earth

Although there are more than a dozen calibrations of AVHRR channels 1 and 2, the difference between calibration methods, the assumptions and corrections used, the data sources and targets all contribute to a wide scatter in calibration values. Table 3 lists a variety of the calibrations available. Figure 1 shows the monthly mean July reflectance from NOAA-9, channel 1 for the Libyan Desert target (28-29° E, 21-23° N) using the

Deleted: 2

calibrations from the sources in table 3. Calibrated reflectances were computed using the mean counts of seven ½ degree averages from GAC data that were centred within the target area. Only fully clear scenes were used in which the solar zenith and satellite view angles were each less than 60 degrees. Clear/cloudy classification was taken from PATMOS-x. The prelaunch calibration is shown for reference. Considering that NOAA-9 has had the most calibration work done and channel 1 on an afternoon satellite is simplest to calibrate, we would expect the agreement to be among the best of all the AVHRRs. The agreement among all but the prelaunch calibration and PALGSFC9596 (Vermote and Kaufman 1995, Vermote and El Saleous 1996), is within about 6 percent reflectance, or 15% relative. Figure 2 is the same as figure 1, but for NOAA-14. The agreement among all calibrations except for prelaunch and Rao (Rao and Chen 1995) is about 7 percent reflectance, or 17% relative. Agreements for the other afternoon satellites are in the 7-17% relative range. The best agreement among channel 1 calibrations tends to be with the most recent afternoon satellites (not shown), most likely due to the orbit stabilization on these later platforms. Calibrations for the morning satellites and channel 2 show a greater lack of agreement. However, many of these calibrations are not from active programs. If we consider only currently active programs that have made their calibrations available at the time of this publication (ISCCP, LTDR, NESDIS, PATMOS-x), we find that the calibrations still differ from each other by around 10% for most of the satellites. Figure 3 shows the slopes for NOAA-16, channel 1 calibrations as a percent difference from the PATMOS-x calibration – this is the best agreement among the current calibrations of any the satellites.

Deleted: 2

## 4. Path Toward Consensus

With the myriad of calibrations and methods out there, how can any AVHRR user decide which one to use? The differences are large enough to make one's choice not trivial, and create lack of confidence in any conclusions drawn from using a single calibration. Certainly, any calibration should have an error small enough to detect known medium-term changes, such as the 3% change in global cloudiness during the 11 year sunspot cycle (Svensmark and Friis-Christensen 1997). At longer time scales, is thought that a calibration with an error level of 1/5$^{th}$ of the expected signal is needed in order to detect climate change. For AVHRR-derived reflectance, for example, that would mean all calibrations would need to agree within 5% relative and have a 1% per decade stability (Ohring et al. 2004). While we recognize that it is impossible to create a single consensus calibration, in this section we argue that it is possible to decrease the errors and increase the agreement among the calibrations produced by the currently active groups such that each will satisfy the requirements of detecting climate change. We present a list of Consensus Items: common data sources, targets, corrections, functions and comparisons that will reduce the scatter among individual calibrations and bring the calibration community toward a set of "consensus" calibrations, that is, calibrations that differ by only an acceptably small amount. They are presented in order of probable ease of agreement and adoption (among the calibration community), easiest first, most difficult last.

The first two Consensus Items are related to converting AVHRR reflectance to or from radiance. When computing a calibration, it is sometimes necessary to convert

between reflectance and radiance. This is done, for example, when comparing AVHRR data to those from another instrument. The conversion between radiance and reflectance requires two important pieces of information: a solar spectrum and the AVHRR spectral response function. The first Consensus Item is a common solar spectrum. Most calibration studies in the past have used some form of the Neckel and Labs (1984) spectrum. Earlier versions of PATMOS-x used one from Kurucz (1995). The Committee on Earth Observation Satellites Working Group on Calibration and Validation (CEOS WGCV) has recommended (CEOS WGCV 2006) that the solar spectrum of Thuillier et al. (2003) be used as the standard spectrum. We recommend that all AVHRR calibration work use this spectrum, which can be downloaded as a spreadsheet from http://www.ceos.org/index.php?option=com_content&view=category&layout=blog&id=95&Itemid=140. Figure 4 shows the Thuillier et al. (2003), the Neckel and Labs (1984) spectrum subsampled by Rossow et al. (1985) and the difference of Thuillier et al. (2003) minus Neckel and Labs (1984) as subsampled by Rossow et al. (1985) in the region of overlapping wavelength. The main advantage of the Thuillier spectrum relative to calibrating AVHRR is that the wavelength resolution is much finer. This allows a more accurate computation of the total incident radiance in each spectral channel, as the absorption bands are better resolved.

The second Consensus Item is the use of a set of corrected spectral response functions (SRFs). As noted previously, there are some errors in the AVHRR SRFs printed in the original documentation. Corrected versions are available at http://www.star.nesdis.noaa.gov/smcd/spb/fwu/solar_cal/spec_resp_func/index.html (Wu 2009). Tables 4 and 5 list the integrated solar amount for channels 1 and 2, respectively, contained in the POD Guide (Kidwell 1998) and KLM Guide (Robel 2009), calculated using the corrected SRFs with the Neckel and Labs (1984) spectrum subsampled by Rossow et al. (1985), and calculated using the corrected SRFs using the Thuillier et al. (2003) spectrum. The integrated solar amount for recommended SRF/spectrum combination difference from the POD/KLM values is 1% to 2% for most of the AVHRRs, but is as large as 8.8% (see tables 4 and 5). Related research investigating how AVHRR spectral response functions change in orbit over time would be very welcome, as little is known about it.

The third Consensus Item is to use a single slope count conversion for calibrating the AVHRR/3s. Personal communication by the authors with the engineers of the AVHRR/3 (see Heidinger et al. 2010) has revealed the algorithm for the gains in the high and low gain regions of the instrument. Simply put, the reflectance:count gain below the switch count should be halved, and that above multiplied by 1.5, which yields a new single-slope count,

$$C = D + 0.5\left(C_{dg} - D\right) \qquad C_{dg} < B_{dg} \qquad (1)$$

$$C = B_{sg} + 1.5\left(C_{dg} - B_{dg}\right) \qquad C_{dg} > B_{dg}, \qquad (2)$$

where $C$ is the single slope absolute count, $D$ is the dual-slope dark count, $C_{dg}$ is the dual-slope absolute count, $B_{dg}$ is the dual-slope switch count and $B_{sg}$ is the single slope count value at the dual-slope switch count. Verification of equations (1) and (2) can be seen in figure 5. Using simultaneous nadir overpasses, the MODIS reflectance, adjusted

Deleted: 2008

Deleted:

Deleted: http://wgcv.ceos.org/

Formatted: Highlight

Deleted: 3

Deleted: 4

Deleted: 3

Deleted: 4

Deleted: 2009

Comment [ccm1]: * deleted and changed variable names to reflect changes made in Heidinger et al companion paper

Comment [ccm2]: * deleted and changed variable names to reflect changes made in Heidinger et al companion paper

for the spectral response of AVHRR, is a linear function of the single-slope converted counts from GAC, with only a small amount of scatter. Converting to a single-slope version of the AVHRR/3 counts will reduce the need for both bright and dark targets, and will remove some of the uncertainty in slopes due to counts averaged around the gain switch.

The fourth Consensus Item is actually a group of items related to calibration targets. We recommend that the calibration community identify and use a common set of targets either directly for calibration, or as a check of the reasonableness of each calibration method. These targets will have agreed-upon reflectances, agreed-upon functions of their reflectance as a function of solar zenith angle and agreed-upon variations in reflectance over short and long time periods. One organization that has begun such an effort is the CEOS Working Group on Calibration and Validation and the Infrared and Optical Visible Sensors subgroup. They have identified several Reference Standard Test Sites: eight instrumented sites and five pseudo-invariant test sites. These can be found at http://calval.cr.usgs.gov/sites_catalog_map.php. These sites are predominantly desert and playa, with one snow and ice field (Dome C). Only one of the sites, La Crau, France, has reflectances near or below 25% (according to the current site questionnaires), so another low reflectance site would be of benefit for calibrating the low slope region of the AVHRR/3 sensors for groups that calibrate the two gains separately.

Deleted: -

Lastly, the fifth Consensus Item is to use simultaneous nadir overpasses (SNOs) of polar orbiting satellites to transfer calibrations from one instrument to another, which would include transferring calibrations between two different NOAA POES satellites (AVHRR/AVHRR), as well as between the NOAA POES and other polar orbiting satellites (e.g., AVHRR/MODIS). Each satellite in any pair of polar orbiting satellites in different orbits (morning/afternoon) will eventually overpass the same point on the Earth within a few seconds or minutes of the other. Kepler's third law implies that the higher the altitude of a satellite, the longer its orbital period. Because satellites at different altitudes have different angular velocities, they must have different orbital periods. Since a lower orbiting satellite (typically a POES morning satellite) has a faster speed than a higher orbiting satellite (typically a POES afternoon satellite), it follows that the satellite orbiting at a lower altitude will eventually pass a satellite orbiting at a higher altitude, creating an SNO. The locations of these SNOs are easily calculated by knowing the two line orbital elements, which are routinely available and using the Simplified General Perturbations Satellite Orbit Model 4 (Lane and Cranford 1969, Hoots and Roehrich 1988) to calculate the exact location of the SNO. Typically, for polar orbiting satellites, these simultaneous overpasses occur in latitudinal bands near the poles. Figure 6 shows an example of the SNO locations for NOAA-17 and NOAA-18 over the course of August 2007.

Using the times of these SNOs we can process and analyze the scenes specific to the SNOs. Because the satellites are flying over the same point on the Earth at nearly the same time, the illumination and the viewing geometry are all essentially equal for the two instruments. If comparing AVHRRs on two NOAA POES satellites, one only needs to account for the different characteristics of the two AVHRR instruments. When comparing the NOAA POES and NASA EOS satellites, in addition to considering the two different instruments' spectral characteristics, one also needs to consider the footprints of each instrument. In order to get around the footprint issue, one remaps the

pixel level data to a consistent equal angle grid. The SNO method has been used in several studies for inter-satellite calibration (e.g., Cao et al. 2004, Cao et al. 2005, Cao and Heidinger 2002, Heidinger et al. 2002). The use of SNOs is particularly advantageous for calibrating AVHRR morning satellites, because the calibration from an easier-to-calibrate afternoon satellite can be transferred to the morning satellite, regardless of illumination angle. Figure 7 shows an example of a calibration derived from SNOs. Here, the combination of the slopes of the NOAA-17 channel 1 raw counts with the derived "true" Libyan Desert and Dome-C reflectances, along with the slopes of the SNO of NOAA-17 with NOAA-15, NOAA-18, Metop-A, Aqua-MODIS and Terra-MODIS are plotted with a best fit curve. The inclusion of SNOs creates a large number of data points with which to derive a statistically robust calibration.

SNOs can also be used to check the satellite-to-satellite calibration consistency. Figure 8 shows monthly mean July reflectance based on NOAA-12 (1992-1998) and NOAA-15 (1999-2008) counts over a northern Greenland target. The ISCCP and PATMOS-x calibrations have been applied. LTDRV3 and NESDISV2T do not have calibrations for these two morning satellites. We can use SNOs to compute a time-dependent count slope between two satellites, that is, the ratio between the two satellites' counts for many scenes over time. Using these slopes, we can convert the counts of a morning satellite, such as NOAA-12 to equivalent counts for an afternoon satellite, such as NOAA-11. Plotting the morning satellite's reflectances using the afternoon satellites' calibrations over time reveals whether a calibration method is consistent from satellite to satellite. Figure 9 shows monthly mean July reflectance based on NOAA-12 (1992-1998) and NOAA-15 (1999-2008) counts over a northern Greenland target. Using SNO count/count slopes, counts were converted to equivalent counts for NOAA-11 (1992-1994), NOAA-14 (1995-2000), NOAA-16 (2001-2002, 2004, 2005), NOAA-17 (2003) and NOAA-18 (2006-2008), and calibrations for these satellites were applied. The calibration consistency is similar to that in the first plot where the morning satellites were calibrated directly, indicating that the ISCCP and PATMOS-x calibrations are about as consistent between satellites as they are for a single satellite. This cross-calibration example also suggests that the ISCCP calibrations for afternoon satellites may be of higher quality than those of the morning satellites. Also, as a benefit, this method allows morning satellite data to be used even if only afternoon satellites have been calibrated, such as with LTDRV3 and NESDISV2T.

We have not explicitly discussed the expected percent improvements for each consensus item in this paper, as the differing calibration methodologies may not show the same amount of improvement by adopting a particular consensus item. However, by virtue of using a core of identical data sets and comparisons, the calibrations will be drawn closer to each other. Any remaining differences will be due purely to the different approaches to calibration and the absolute reflectance standards used, if any. In a companion paper to this one, Heidinger et al. (2010) have used these consensus items in their calibration of ch1 and ch2 on all AVHRRS from TIROS-N through NOAA-19. The analysis of uncertainty in that paper concludes that their calibration is accurate to within 2 % and 3 % relative to MODIS. We conclude here that using the consensus items listed here would produce a similar amount of error relative to the chosen standard, allowing another 2-3 % relative difference of freedom between standards and methodologies to

Deleted: 2009

satisfy the 5% relative agreement required for climate studies. This seems entirely reasonable.

## 5. Remaining Issues

To make the most of the AVHRR record, an uninterrupted time series of data is needed. At this time, there are many gaps in NOAA's Comprehensive Large Array-data Stewardship System (CLASS, http://www.class.ngdc.noaa.gov/saa/products/welcome) collection of AVHRR data in GAC and LAC/HRPT formats, mostly for the early satellites. An effort should be made to search all possible archives that may have any of the missing data, so that these data may be uploaded to the CLASS and available for all AVHRR users. Perhaps disseminating a list of missing imagery from the CLASS web site would encourage researchers to examine their collections for these missing data.

Deleted: n

## 6. Conclusions

The objective of this paper was to review all the issues related to calibrating the solar channels of the AVHRR and to outline a path forward so that the calibration community can work toward a set of calibrations that are within close enough agreement as to be considered a consensus. The currently available calibrations cannot be said to agree closely enough for long term climate studies. Although the calibration challenges listed are many for AVHRR, there are several data sources and methodologies that can bring the calibration community into effective consensus: a common solar spectrum, corrected spectral response functions, converting AVHRR/3 counts to a single slope count, using CEOS WGCV's Reference Standard Test Sites, and using simultaneous nadir overpasses to transfer calibrations from one instrument to another. We recommend that the AVHRR calibration community adopt these Consensus Items in their calibration protocols and work together toward filling in gaps in the CLASS AVHRR archive in order to enable the AVHRR solar channel data to be exercised in the way it truly deserves.

## 7. Acknowledgements

We thank the members of the AVHRR calibration community who shared their most recent efforts with us and answered all of our questions. We also wish to thank the anonymous reviewers for their helpful suggestions that improved this paper. This work was funded by NOAA grant NA07OAR4310199.

The views, opinions, and findings contained in this report are those of the author(s) and should not be construed as an official National Oceanic and Atmospheric Administration or U.S. Government position, policy, or decision.

## 8. References

BREST, C.L. and ROSSOW, W.B., 1992, Radiometric calibration and monitoring of NOAA AVHRR data for ISCCP. *International Journal of Remote Sensing,* **13**, pp. 235-273.

BREST, C.L., ROSSOW, W.B. and ROITER, M.D., 1997, Update of radiance calibrations for ISCCP. *Journal of Atmospheric and Oceanic Technology,* **14**, pp. 1091-1109.

CAO, C. and HEIDINGER, A.K., 2002, Intercomparison of the longwave infrared channels of MODIS and AVHRR/NOAA-16 using simultaneous nadir observations at orbit intersections. In *Proceedings of Earth Observing Systems VII*, 24 September 2002 (Bellingham, WA: SPIE), Vol. 4814, pp. 306–316.

CAO, C., WEINREB, M. and XU, H., 2004, Predicting simultaneous nadir overpasses among polar-orbiting meteorological satellites for the intersatellite calibration of radiometers. *Journal of Atmospheric and Oceanic Technology*, **21**, pp. 537–542.

CAO, C., XU, H., SULLIVAN, J., MCMILLIN, L., CIREN, P. and HOU, Y., 2005, Intersatellite radiance biases for the high resolution infrared radiation sounders (HIRS) onboard NOAA-15, -16 and -17 from simultaneous nadir observations. *Journal of Atmospheric and Oceanic Technology*, **22**, pp. 381-395.

CEOS WGCV (Committee on Earth Observation Satellites Working Group on Calibration and Validation), 2006, Use of exo-atmospheric solar spectral irradiance (200 to 2400 nm). Available online at: http://www.ceos.org/images/WGCV/wgcv26/solirrad.pdf (accessed 05 May 2010).

CIHLAR, J. and TEILLET, P.M., 1995, Forward piecewise linear calibration model for quasi-real time processing of AVHRR data. *Canadian Journal of Remote Sensing*, **21**, pp. 22-27.

CIHLAR, J., LATIFOVIC, R., CHEN, J., TRISHCHENKO, A., DU, Y., FEDOSEJEVS, G. and GUINDON, B., 2004, Systematic corrections of AVHRR image composites for temporal studies. *Remote Sensing of Environment*, **89**, pp. 217-233.

CHE, N. and PRICE, J.C., 1992, Survey of radiometric calibration results and methods for visible and near infrared channels of NOAA-7, -9 and -11 AVHRRs. *Remote Sensing of Environment*, **41**, pp. 19-27.

CRACKNELL, A.P., 1997, *The Advanced Very High Resolution Radiometer* (London: Taylor and Francis).

DOELLING, D.R., CHAKRAPANI, V., MINNIS, P. and NGUYEN, L., 2001, The calibration of NOAA-AVHRR visible radiances with VIRS. In *Proceedings of the 11th Conference on Satellite Meteorology and Oceanography*, 15-18 October 2001, Madison, WI (Boston: American Meteorological Society), pp. 614-617.

DOELLING, D.R., GARBER, D.P., AVEY, L.A., NGUYEN, L. and MINNIS, P., 2007, The calibration of AVHRR visible dual gain using Meteosat-8 for NOAA-16 to 18. In *Proceedings of SPIE Conference on Atmospheric and Environmental Remote Sensing Data Processing and Utilization III: Readiness for GEOSS*, 27 August 2007, San Diego, CA (Bellingham, WA: SPIE), Vol. 6684, 668409 CD-ROM.

DOELLING, D.R., NGUYEN, L. and MINNIS, P., 2004, On the use of deep convective clouds to calibrate AVHRR data. In *Earth Observing Systems IX,* 2-6 August 2004, Denver, CO (Bellingham, WA: SPIE), Vol. 5542, pp. 281-289.

FROUIN, R. and GAUTIER, C., 1987, Calibration of NOAA-7 AVHRR, GOES-5 and GOES-6 VISSR/VAS solar channels. *Remote Sensing of Environment,* **22**, pp. 73-101.

HEIDINGER, A.K., CAO, C. and SULLIVAN, J.T., 2002, Using moderate resolution imaging spectrometer (MODIS) to calibrate advanced very high resolution radiometer reflectance channels. *Journal of Geophysical Research,* **107**, pp. 11.1-11.9.

HEIDINGER, A.K. and STRAKA, W.C., 2009, CIMSS CLAVR Home Page. Available at: http://cimss.ssec.wisc.edu/clavr/ (accessed 29 April 2010).

HEIDINGER, A.K., STRAKA III, W.C., MOLLING, C.C., and SULLIVAN, J.T., 2010, Deriving an inter-sensor consistent calibration for the AVHRR solar reflectance data record. *International Journal of Remote Sensing* (companion paper).

HEINZMANN, U., 1993, Analysis of cloud type and distribution using NOAA AVHRR APT data and ground observations in the upper Rhine valley. *Proceedings of Geoscience and*

Deleted: 2008
Deleted: http://wgcv.ceos.org/docs/plenary/wgcv26/Solirrad.pdf
Deleted: 06 July 2009
Formatted: Highlight
Formatted: Highlight
Deleted: 06 July 2009
Deleted: PAVOLONIS, M.J.
Deleted: Y
Deleted: 2009
Formatted: Highlight
Formatted: Font: 11 pt
Formatted: Font: 11 pt
Formatted: Font: Italic

*Remote Sensing Symposium, 1993, IGARSS '93, Better Understanding of Earth Environment., International*, 18-21 August 1993, Tokyo, Japan (New York, NY: IEEE), **4**, pp. 1821-1823.

HOOTS, F.R. and ROEHRICH, R.L., 1988. Models for propagation of NORAD element sets. Aerospace Defense Command Spacetrack Report 3, Peterson AFB, CO, 90 pp.

KAUFMAN, Y.J. and HOLBEN, B.N., 1993. Calibration of the AVHRR visible and near-IR bands by atmospheric scattering, ocean glint and desert reflection. *International Journal of Remote Sensing*, **14**, pp. 21-52.

KIDWELL, K.B. (Ed.), 1998, *NOAA Polar Orbiter Data User's Guide*. Available online at: http://www.ncdc.noaa.gov/oa/pod-guide/ncdc/docs/podug/index.htm (accessed 29 April 2010).

KURUCZ, R.L., 1995, The solar irradiance by computation. In *Proceedings of the 17th Annual Conference on Atmospheric Transmission Models*, 8-9 June 1994, Hanscom Air Force Base, MA (Hanscom AFB: Phillips Laboratory), pp. 333-334.

LANE, M.H. and CRANFORD, K.H., 1969, An improved analytical drag theory for the artificial satellite problem. American Institute of Aeronautics and Astronautics Paper 1969-925, (Reston, VA: AIAA).

LATIFOVIC, R., TRISHCHENKO, A.P., CHEN, J., PARK, W.B., KHLOPENKOV, K.V., Fernandez, R., POULIOT, D., UNGUREANU, C., LUO, Y., WANG, S., DAVIDSON, A. and CIHLAR, J., 2005, Generating historical AVHRR 1 km baseline satellite data records over Canada suitable for climate change studies. *Canadian Journal of Remote Sensing*, **31**, pp. 324-346.

LOEB, N.G., 1997, In-flight calibration of NOAA AVHRR visible and near-IR bands over Greenland and Antarctica. *International Journal of Remote Sensing*, **18**, pp. 477-490.

MASONIS, S.J. and WARREN, S.G., 2001, Gain of the AVHRR visible channel as tracked using bidirectional reflectance of Antarctic and Greenland snow. *International Journal of Remote Sensing*, **22**, pp. 1495-1520.

NECKEL, H. and LABS, D., 1984, The solar radiation between 3300 and 12500 angstroms. *Solar Physics*, **90**, pp. 205-258.

NGUYEN, L., DOELLING, D.R., MINNIS, P. and AYERS, J.K., 2004, Rapid technique to cross calibrate satellite imager visible channels. In *Earth Observing Systems IX,* 2-6 August 2004 Denver, CO (Bellingham WA: SPIE), Vol. 5542, pp. 227-235.

OHRING, G., WIELICKI, B., SPENCER, R., EMERY, B. and DATLA, R., 2004, Satellite instrument calibration for measuring global climate change. National Institute of Standards and Technology Internal Report NISTIR 7047 (Washington D.C.: NIST).

RAO, C.R.N. and CHEN, J., 1995, Inter-satellite calibration linkages for the visible and near-infrared channels of the advanced very high resolution radiometer on the NOAA-7, -9 and -11 spacecraft. *International Journal of Remote Sensing,* **16**, pp. 1931-1942.

RAO, C.R.N. and CHEN, J., 1996, Post-launch calibration of the visible and near-infrared channels of the advanced very high resolution radiometer on the NOAA-14 spacecraft. *International Journal of Remote Sensing,* **17**, pp. 2743-2747.

ROBEL, J. (Ed.), 2009, *NOAA KLM User's Guide with NOAA-N, -N' Supplement*. Available online at: http://www.ncdc.noaa.gov/oa/pod-guide/ncdc/docs/klm/index.htm (accessed 29 April 2010).

ROSSOW, W. B., KINSELLA, E., WOLF, A. and GARDNER, L., 1985. International Cloud Climatology Project description of reduced resolution radiance data. World Meteorological Organization Technical Document No. 58, 132 pp.

SMITH, G.R., LEVIN, R.H., ABEL, P. and JACOBOWITZ, H., 1988, Calibration of the solar channels of the NOAA-9 AVHRR using high altitude aircraft measurements. *Journal of Atmospheric and Oceanic Technology*, **5**, pp. 631-639.

Formatted: Font: Italic
Formatted: Font: Bold
Formatted: Font: 11 pt
Deleted: 06
Deleted: July
Deleted: 2009
Deleted: 06
Deleted: July
Deleted: 09

STAYLOR, W.F., 1990, Degradation rates of the AVHRR visible channel for the NOAA 6, 7 and 9 spacecraft. *Journal of Atmospheric and Oceanic Technology*, **7**, pp. 411-423.

SVENSMARK, H. and FRIIS-CHRISTENSEN, E., 1997, Variation of cosmic ray flux and global cloud coverage – a missing link in solar-climate relationships. *Journal of Atmospheric and Solar-Terrestrial Physics*, **59**, pp. 1225-1232.

TAHNK, W.R. and COAKLEY Jr., J.A., 2001a, Improved calibration coefficients for NOAA-14 AVHRR visible and near-infrared channels. *International Journal of Remote Sensing*, **22**, pp. 1269-1283.

TAHNK, W.R. and COAKLEY Jr., J.A., 2001b, Updated calibration coefficients for NOAA-14 AVHRR channels 1 and 2. *International Journal of Remote Sensing*, **22**, pp. 3053-3057.

TAHNK, W.R. and COAKLEY Jr., J.A., 2002, Improved calibration coefficients for NOAA-12 and NOAA-15 AVHRR visible and near-IR channels. *Journal of Atmospheric and Oceanic Technology*, **19**, pp. 1826-1833.

THUILLIER, G., HERSÉ, M., LABS, D., FOUJOLS, T., PEETERMANS, W., GILLOTAY, D., SIMON, P.C. and MANDEL, H., 2003, The solar spectral irradiance from 200 to 2400 nm as measured by the SOLSPEC spectrometer from the Atlas and Eureca missions. *Solar Physics*, **214**, pp. 1-22.

VERMOTE, E. and KAUFMAN, Y.J., 1995, Absolute calibration of AVHRR visible and near-infrared channels using ocean and cloud views. *International Journal of Remote Sensing*, **16**, pp. 2317-2340.

VERMOTE, E. and EL SALEOUS, N., 1996, Absolute calibration of AVHRR channels 1 and 2. In *Advances in the Use of NOAA AVHRR Data for Land Applications*, G. D'Souza, A.S. Belward and J.-P. Malingreau (Eds.), pp. 73-92, (Boston: Kluwer).

VERMOTE, E. and EL SALEOUS, N., 2006, Calibration of NOAA-16 over a desert site using MODIS data. *Remote Sensing of Environment*, **105**, pp. 214-220.

WILLSON, R.C. and MORDVINOV, A.V., 2003, Secular total solar irradiance trend during solar cycles 21–23. Geophysical Research Letters, **30**, 1199, doi:10.1029/2002GL016038.

WU, X., 2004, Operational calibration of solar reflectance channels of the advanced very high resolution radiometer (AVHRR). In *Earth Observing Systems IX,* 2-6 August 2004, Denver, CO (Bellingham, WA: SPIE), Vol. 5542, pp. 272-280.

WU, X., 2009, NOAA AVHRR spectral response functions. Available online at: http://www.star.nesdis.noaa.gov/smcd/spb/fwu/solar_cal/spec_resp_func/index.html (accessed 29 April 2010).

Deleted: 06

Deleted: July

Deleted: 2009

## 9. Tables

Table 1. Launch date (dd mon yyyy) of polar orbiting satellites that bore operational AVHRRs, along with service dates and the times (local standard time) of the ascending and descending nodes of the orbit at launch.

| Satellite | Launch Date | Start Date | End Date | Ascending Node | Descending Node |
|---|---|---|---|---|---|
| TIROS-N | 13 Oct 1978 | 19 Oct 1978 | 30 Jan 1980 | 1500 | 0300 |
| NOAA-6 | 27 Jun 1979 | 27 Jun 1979 | 16 Nov 1986 | 1930 | 0730 |
| NOAA-7 | 23 Jun 1981 | 19 Aug 1981 | 07 Jun 1986 | 1430 | 0230 |
| NOAA-8 | 28 Mar 1983 | 20 Jun 1983 | 12 Jun 1984 | 1930 | 0730 |
| | | 01 Jul 1985 | 31 Oct 1985 | | |
| NOAA-9 | 12 Dec 1984 | 25 Feb 1985 | 07 Nov 1988 | 1420 | 0220 |
| NOAA-10 | 17 Sep 1986 | 17 Nov 1986 | 16 Sep 1991 | 1930 | 0730 |
| NOAA-11 | 24 Sep 1988 | 08 Nov 1988 | 11 Apr 1995 | 1330 | 0130 |
| NOAA-12 | 14 May 1991 | 17 Sep 1991 | 14 Dec 1998 | 1930 | 0730 |
| NOAA-14 | 20 Dec 1994 | 11 Apr 1995 | 23 May 2007 | 1330 | 0130 |
| NOAA-15 | 13 May 1998 | 15 Dec 1998 | present | 1930 | 0730 |
| NOAA-16 | 21 Sep 2000 | 20 Mar 2001 | present | 1400 | 0200 |
| NOAA-17 | 24 Jun 2002 | 15 Oct 2002 | present | 2200 | 1000 |
| NOAA-18 | 20 May 2005 | 30 Aug 2005 | present | 1400 | 0200 |
| NOAA-19 | 06 Feb 2009 | 02 Jun 2009 | present | 1400 | 0200 |
| Metop-A | 19 Oct 2006 | 28 Nov 2006 | present | 2130 | 0930 |

Deleted: /mm/
Deleted: /10/
Deleted: /10/
Deleted: /01/
Deleted: /06/
Deleted: /06/
Deleted: /11/
Deleted: /06/
Deleted: /08/
Deleted: /06/
Deleted: /03/
Deleted: /06/
Deleted: /06/
Deleted: /07/
Deleted: /10/
Deleted: /12/
Deleted: /02/
Deleted: /11/
Deleted: /09/
Deleted: /11/
Deleted: /09/
Deleted: /09/
Deleted: /11/
Deleted: /04/
Deleted: /05/
Deleted: /09/
Deleted: /12/
Deleted: /12/
Deleted: /04/
Deleted: /05/
Deleted: /05/
Deleted: /12/
Deleted: /09/
Deleted: /03/
Deleted: /06/
Deleted: /10/
Deleted: /05/
Deleted: /08/
Deleted: /02/
Deleted: /06/
Deleted: /10/
Deleted: /11/

Table 2. A summary of characteristics of the AVHRRs on NOAA and Metop polar orbiting satellites. *Note: Channel 3a senses a mix of solar and Earth emitted wavelengths. Channel 3b is equivalent to channel 3 on non-AVHRR/3 instruments.

| | AVHRR | AVHRR/1 | AVHRR/2 | AVHRR/3 |
|---|---|---|---|---|
| Channels | 1, 2, 3, 4 | 1, 2, 3, 4 | 1, 2, 3, 4, 5 | 1, 2, 3a, 3b, 4, 5 |
| Solar Channels | 1, 2 | 1, 2 | 1, 2 | 1, 2, 3a* |
| Thermal Channels | 3, 4 | 3, 4 | 3, 4, 5 | 3a*, 3b, 4, 5 |
| Channel 1 wavelengths (µm) | 0.55-0.90 | 0.58-0.68 | 0.58-0.68 | 0.58-0.68 |
| Channel 2 wavelengths (µm) | 0.725-1.10 | 0.725-1.10 | 0.725-1.10 | 0.725-1.00 |
| Gain | Single | Single | Single | Dual |
| Footprint at nadir (km) | 1.1 | 1.1 | 1.1 | 1.1 |
| Platforms | TIROS-N | NOAA-6, -8, -10 | NOAA-7, -9, -11, -12, -14 | NOAA-15, -16, -17, -18, -19, Metop-A |

Formatted: Justified

Table 3. Calibrations used in this paper whose values are published in the literature, published on web sites, or provided to authors of this paper.

| Calibration | Reference | Satellites | Channels |
|---|---|---|---|
| Prelaunch | Kidwell 1998, Robel 2009 | 5-13, 14-18 | 1, 2 |
| Rao | Rao and Chen 1995, 1996 | 7, 9, 11, 14 | 1, 2 |
| NESDISv2 | www.osdpd.noaa.gov/ml/ppp/index.html | 7, 9, 11,14, 16, 17, 18 | 1, 2 |
| NESDISv3 | Wu, Xiangqian 2008 (personal communication, Xiangqian.Wu@noaa.gov) | 7, 9, 11,14, 16, 18 | 1 |
| UWash | Masonis and Warren 2001 | 9, 10, 11 | 1 |
| ISCCP | isccp.giss.nasa.gov | 7-12, 14-17 | 1 |
| CCRS/EODM | Latifovic et al. 2005 | 6-12, 14-17 | 1, 2 |
| PALGSFC93 | Kaufman and Holben 1993 | 7, 9, 11 | 1, 2 |
| PALGSFC9596 | Vermote and Kaufman 1995, Vermote and El Saleous 1996 | 7, 9, 11 | 1 |
| LTDRv3 | Vermote and El Saleous 2006, ltdr.nascom.nasa.gov/ltdr/ltdr.html | 7, 9, 11, 14 | 1, 2 |
| PATMOS-x | Heidinger and Straka 2009, Heidinger et al. 2010 | 7-12, 14-17 | 1, 2 |
| LARCVIRS | Nguyen et al. 2004 | 14 | 1 |
| LARCMODIS | Doelling et al. 2004 | 16, 17 | 1, 2 |
| OSU | Tahnk and Coakley 2001a, 2001b, 2002 | 12, 14, 15 | 1, 2 |

Deleted: 2

Deleted: PSB

Deleted: PPP

Deleted: PPP

Deleted: , www.ccrs.nrcan.gc.ca/optic/calval/index_e.php

Deleted: 2009

Table 4. Integrated solar amounts (W $m^{-2}$) for AVHRR channel 1 taken from the POD and KLM Guides (Kidwell 1998, Robel 2009); calculated using corrected spectral response functions (Wu 2009) with the Neckel and Labs (1984) spectrum subsampled by Rossow et al. (1985); and calculated using the corrected SRFs with the Thuillier et al. (2003) spectrum. The percent difference is between the recommended SRFs with the Thuillier spectrum and the values in the POD and KLM Guides.

| Satellite | Original Integrated Solar Kidwell 1998, Robel 2009 (W $m^{-2}$) | Integrated Solar Wu 2009, Rossow et al. 1985 (W $m^{-2}$) | Recommended Integrated Solar Wu 2009, Thuillier et al. 2003 (W $m^{-2}$) | Difference between Recommended and Original (%) |
|---|---|---|---|---|
| TIROS-N | 443.3 | 448.8 | 443.7 | 0.09 |
| NOAA-6 | 179.0 | 180.8 | 177.7 | -0.73 |
| NOAA-7 | 177.5 | 178.1 | 175.1 | -1.37 |
| NOAA-8 | 183.4 | 183.5 | 180.5 | -1.61 |
| NOAA-9 | 191.3 | 191.3 | 188.5 | -1.49 |
| NOAA-10 | 178.8 | 178.8 | 175.7 | -1.76 |
| NOAA-11 | 184.1 | 184.2 | 181.4 | -1.49 |
| NOAA-12 | 200.1 | 200.6 | 197.6 | -1.27 |
| NOAA-14 | 221.4 | 206.5 | 203.5 | -8.80 |
| NOAA-15 | 138.7 | 140.5 | 138.0 | -0.51 |
| NOAA-16 | 133.2 | 134.3 | 132.0 | -0.91 |
| NOAA-17 | 136.2 | 143.1 | 140.5 | 3.06 |
| NOAA-18 | 130.3 | 132.9 | 130.6 | 0.23 |
| NOAA-19 | 126.8 | 126.9 | 124.7 | -1.66 |
| Metop-A | 139.9 | 139.9 | 137.4 | -1.79 |

Table 5. Integrated solar amounts (W $m^{-2}$) for AVHRR channel 2 taken from the POD and KLM Guides (Kidwell 1998, Robel 2009); calculated using corrected spectral response functions (Wu 2009) with the Neckel and Labs (1984) spectrum subsampled by Rossow et al. (1985); and calculated using the corrected SRFs with the Thuillier et al. (2003) spectrum. The percent difference is between the recommended SRFs with the Thuillier spectrum and the values in the POD and KLM Guides.

| Satellite | Original Integrated Solar Kidwell 1998, Robel 2009 (W $m^{-2}$) | Integrated Solar Wu 2009, Rossow et al. 1985 (W $m^{-2}$) | Recommended Integrated Solar Wu 2009, Thuillier et al. 2003 (W $m^{-2}$) | Difference between Recommended and Original (%) |
|---|---|---|---|---|
| TIROS-N | 313.5 | 315.1 | 308.3 | -1.69 |
| NOAA-6 | 233.7 | 234.1 | 229.6 | -1.79 |
| NOAA-7 | 261.9 | 262.0 | 256.8 | -1.99 |
| NOAA-8 | 242.8 | 242.6 | 238.1 | -1.97 |
| NOAA-9 | 251.8 | 252.1 | 247.2 | -1.86 |
| NOAA-10 | 231.5 | 231.9 | 227.2 | -1.89 |
| NOAA-11 | 241.1 | 241.5 | 236.9 | -1.77 |
| NOAA-12 | 229.9 | 230.3 | 225.9 | -1.77 |
| NOAA-14 | 252.3 | 251.5 | 246.2 | -2.48 |
| NOAA-15 | 235.4 | 241.7 | 236.6 | 0.51 |
| NOAA-16 | 243.1 | 243.3 | 237.9 | -2.19 |
| NOAA-17 | 240.6 | 250.5 | 245.1 | 1.84 |
| NOAA-18 | 246.0 | 255.9 | 250.1 | 1.64 |
| NOAA-19 | 225.7 | 229.0 | 224.6 | -0.49 |
| Metop-A | 232.9 | 236.7 | 231.6 | -0.56 |

## 10. Figures

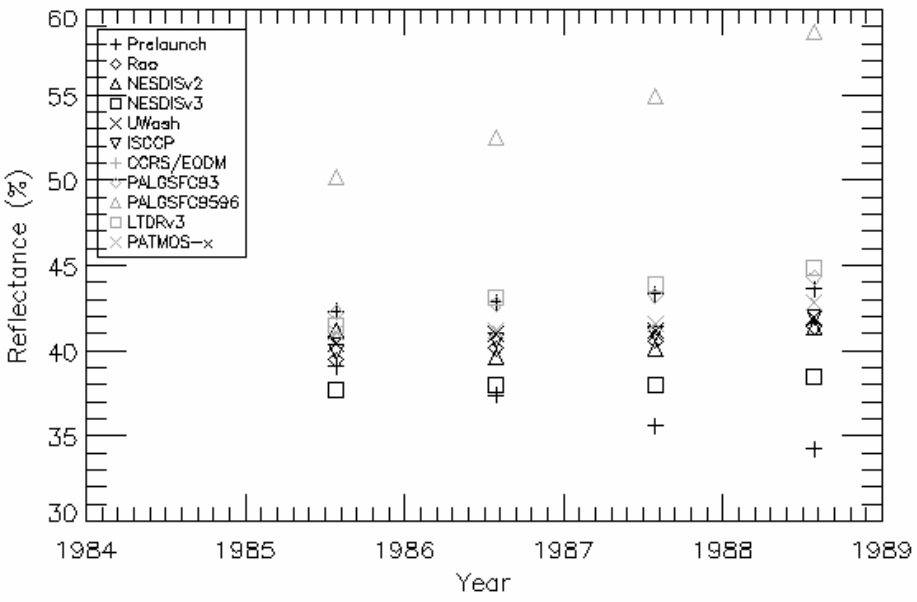


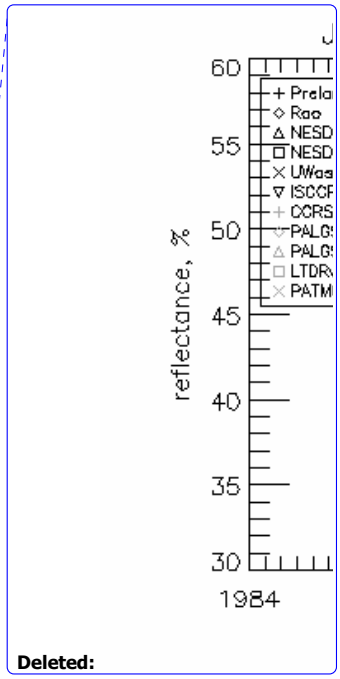


Deleted:

Figure 1. AVHRR channel 1 July mean reflectance for a target in the Libyan Desert. NOAA-9 channel 1 was selected because it shows, except for the PALGSFC9596 calibration, (relatively) good agreement compared to the rest of the satellites/channels for which there are many available calibrations in the literature. A key to the calibrations can be found in table 2.

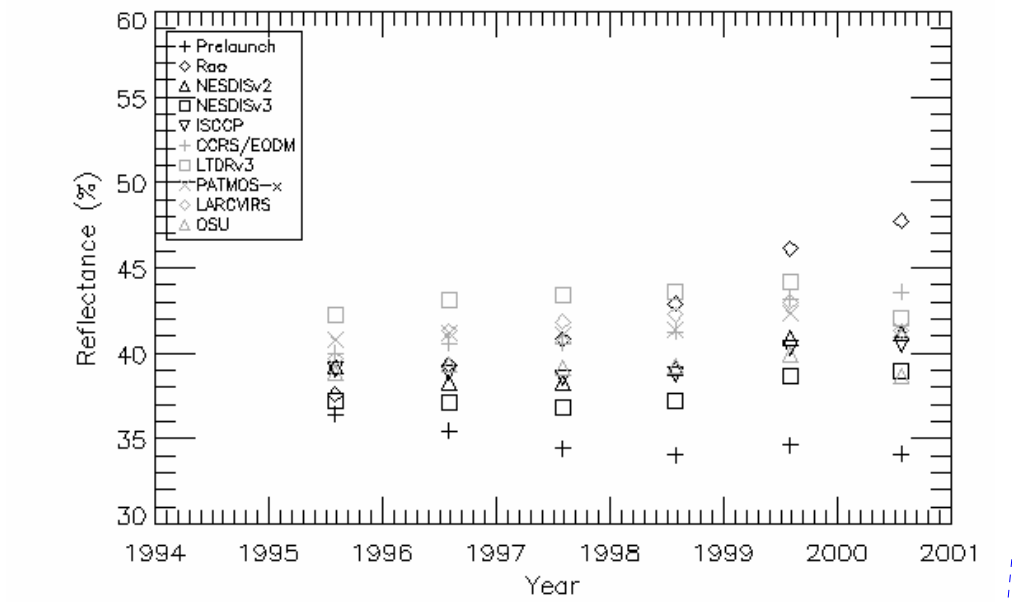


Figure 2. Same as figure 1, but for NOAA-14. NOAA-14 was selected because its calibrations are in (relatively) poor agreement compared to the rest of the satellites/channels for which there are many available calibrations in the literature.

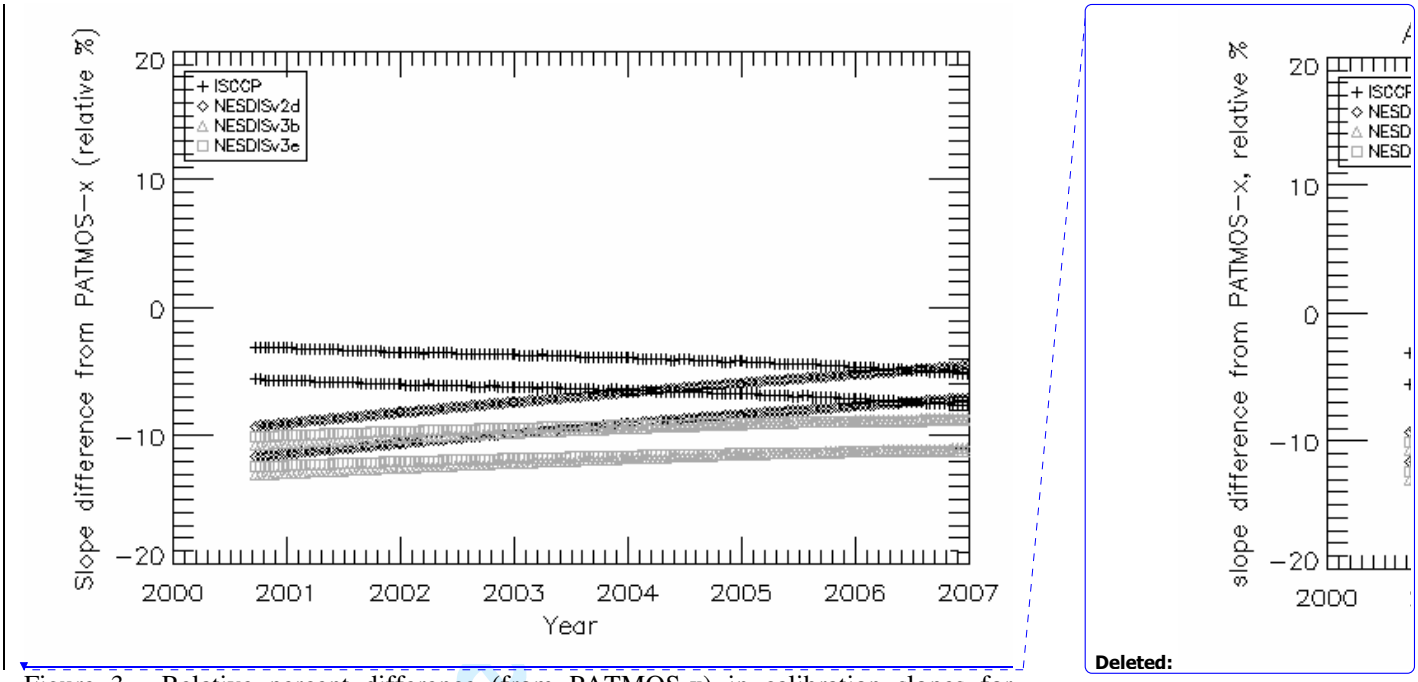


Figure 3. Relative percent difference (from PATMOS-x) in calibration slopes for AVHRR on NOAA-16, channel 1.

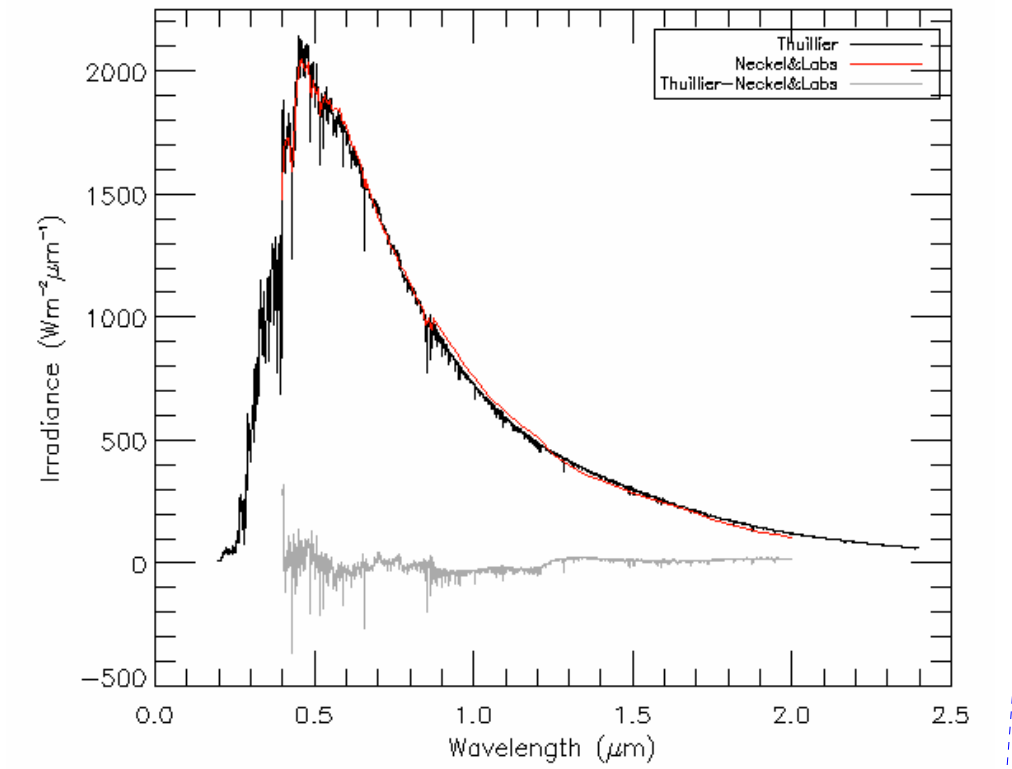


Figure 4. Solar irradiance spectra from Thuillier et al. (2003), black line, Neckel and Labs (1984) as subsampled by Rossow et al. (1985), red line, and the difference in the region of overlapping wavelength, grey line.

Deleted:

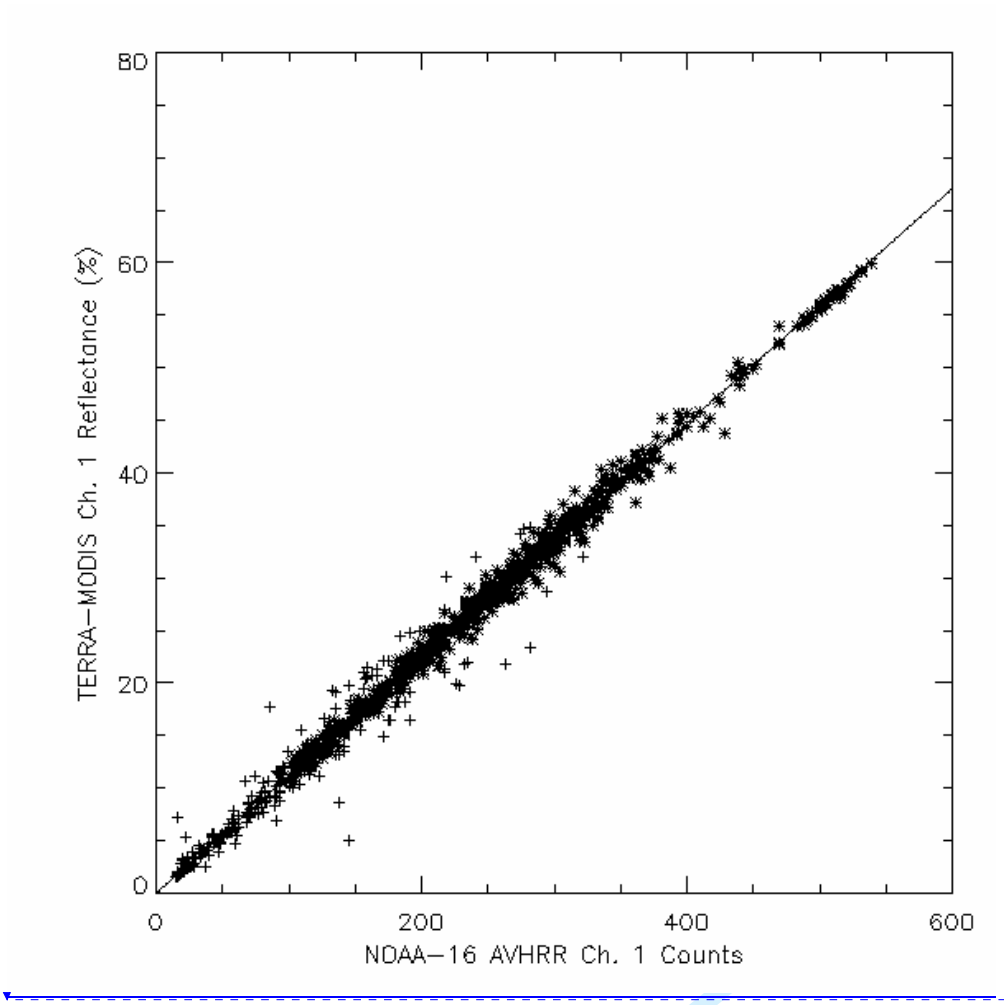


Figure 5. Dual slope counts from channel 1, NOAA-16 AVHRR GAC converted to single slope, then plotted against Terra-MODIS adjusted reflectance for all SNOs during July 2001. The fitted line is $R = 0.111757C$, where $R$ is the reflectance in % and $C$ is the single-slope count.

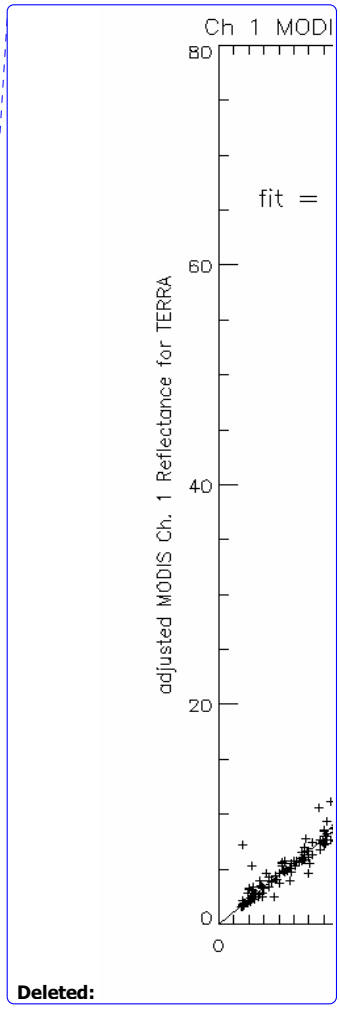


Deleted:

Formatted: Lowered by 3 pt

Formatted: Lowered by 2 pt

Formatted: Lowered by 3 pt

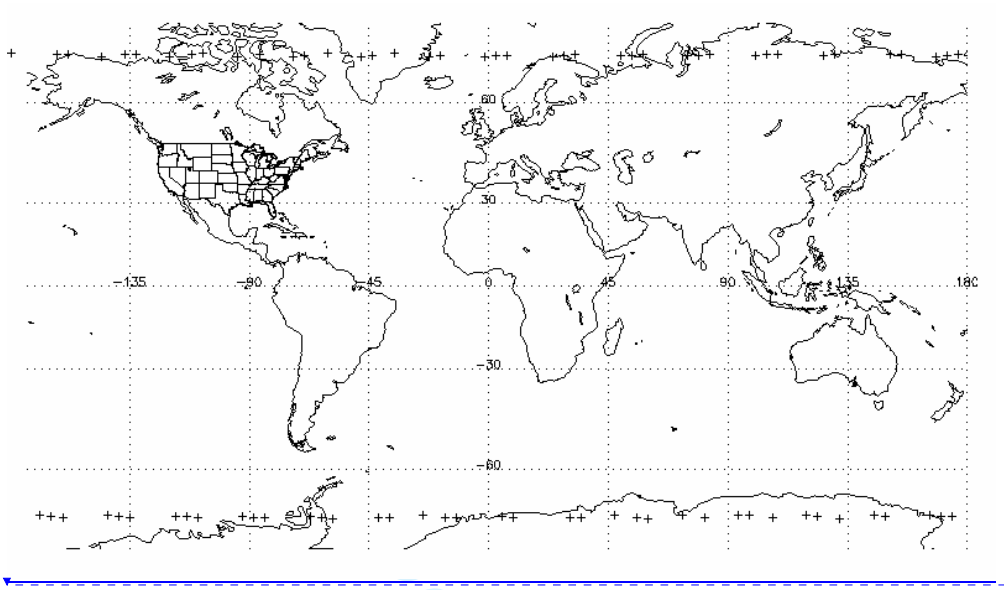


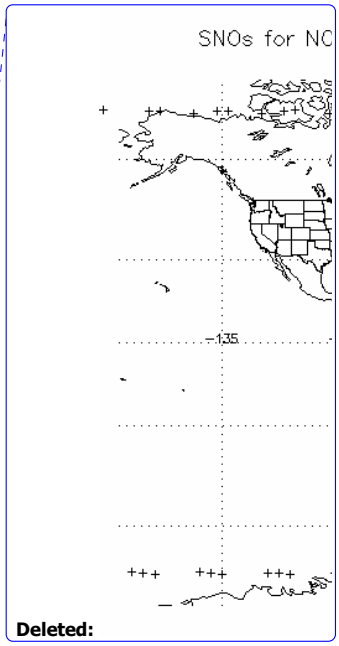


Deleted:

Figure 6. Simultaneous Nadir Overpasses (plus symbols) for NOAA-18 and NOAA-17 during August 2007. SNOs for polar orbiting spacecraft occur in bands near the poles, yielding simultaneous views which may be ocean, ice, cloud or land.

Deleted: for

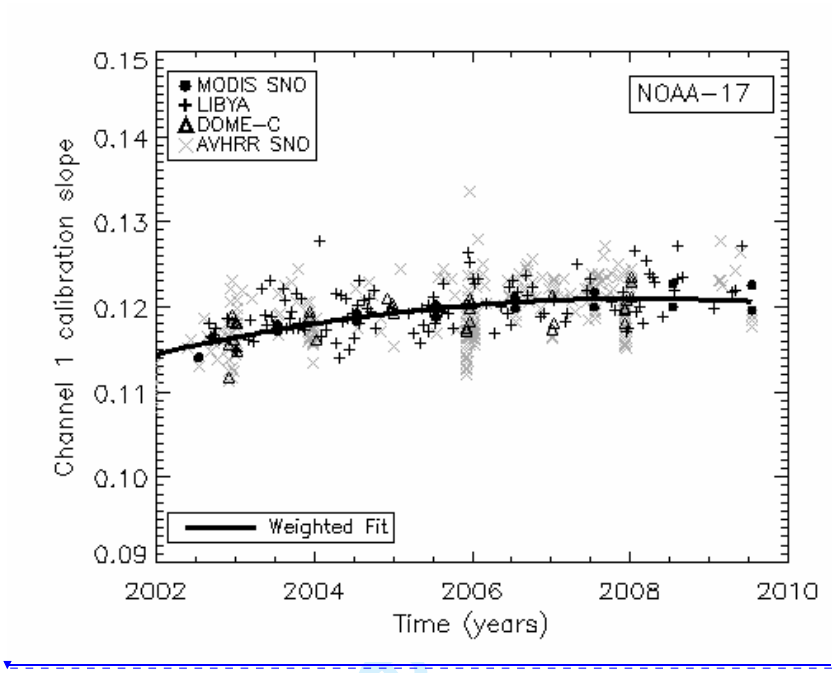


Figure 7. A calibration for NOAA-17, channel 1 derived using constant target reflectances for Libya and Dome-C and simultaneous nadir overpasses between NOAA-17 and NOAA-15, NOAA-18, Metop-A, Aqua-MODIS and Terra-MODIS. The weighted fit line is $S(t) = 0.115(100 + 1.71t + -0.15t^2)/100$, where $S$ is the calibration slope represented by the line and $t$ is time in years since launch. The bias (%) and standard deviation from the mean (%) are listed individually for the calibration data sources and for the data sources as a group.

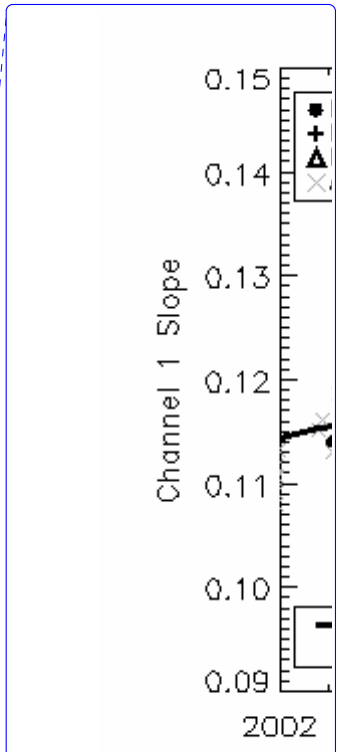


Deleted:
Deleted:
Formatted: Lowered by 5 pt
Formatted: Lowered by 3 pt
Formatted: Lowered by 3 pt

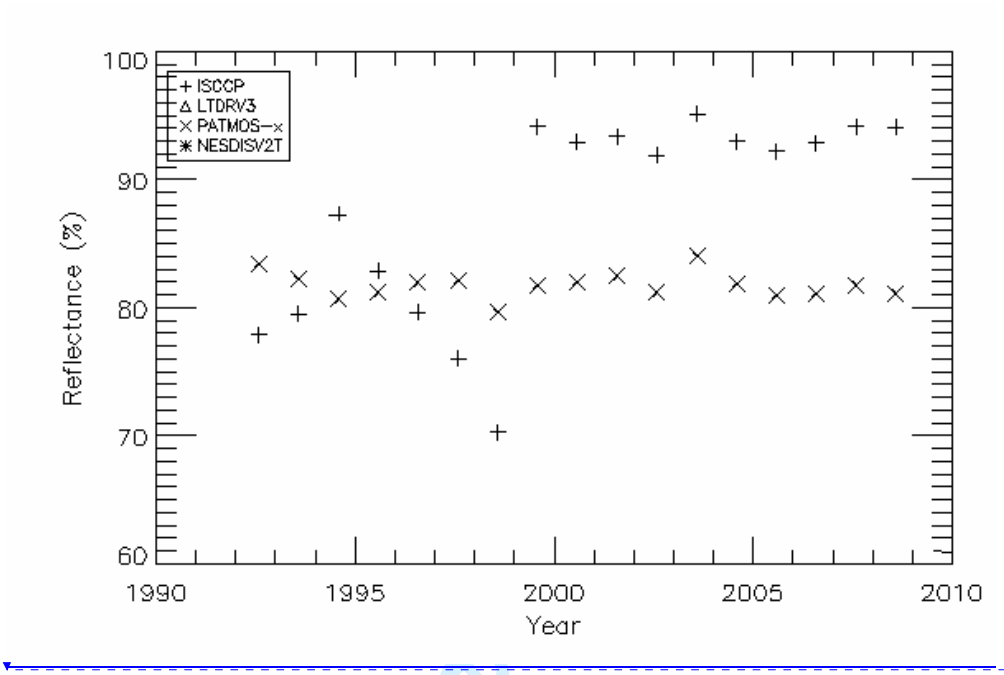


Deleted:

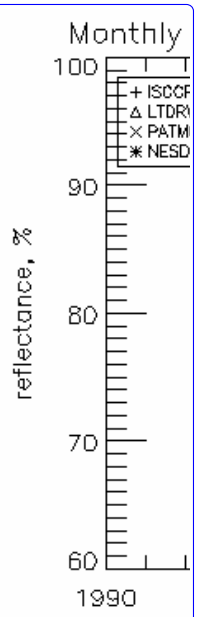


Figure 8. Monthly mean July reflectance based on NOAA-12 (1992-1998) and NOAA-15 (1999-2008) counts over a northern Greenland target. The ISCCP and PATMOS-x calibrations have been applied. LTDRV3 and NESDISV2T do not have calibrations for these two morning satellites.

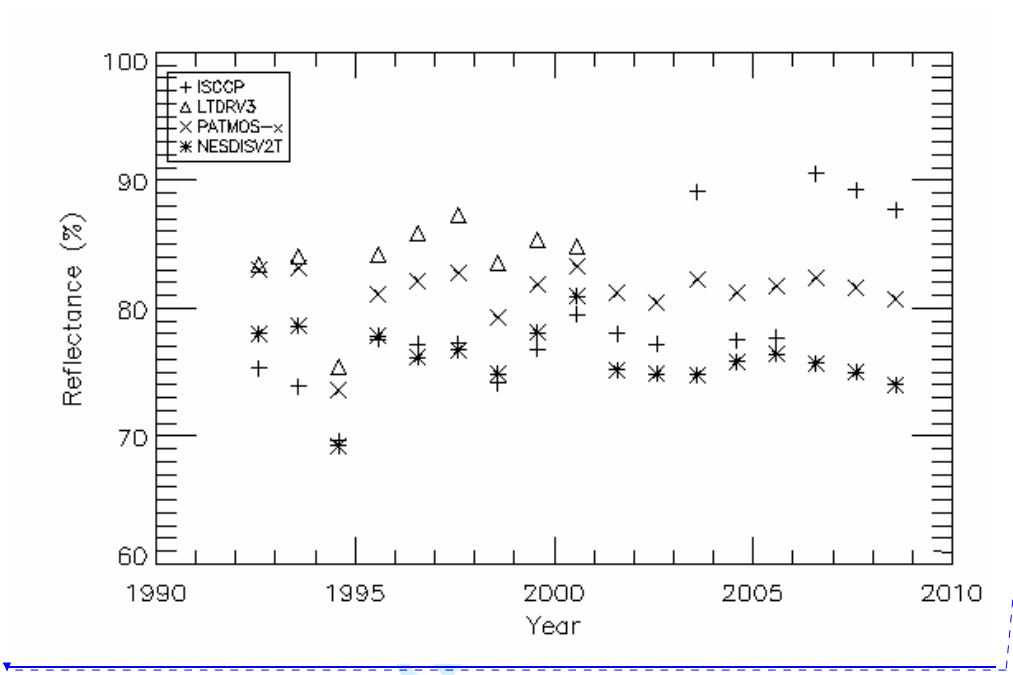


Figure 9. Monthly mean July reflectance based on NOAA-12 (1992-1998) and NOAA-15 (1999-2008) counts over a northern Greenland target. Using SNO count/count slopes, counts were converted to equivalent counts for NOAA-11 (1992-1994), NOAA-14 (1995-2000), NOAA-16 (2001-2002, 2004, 2005), NOAA-17 (2003) and NOAA-18 (2006-2008), and calibrations for these satellites were applied.

Deleted:

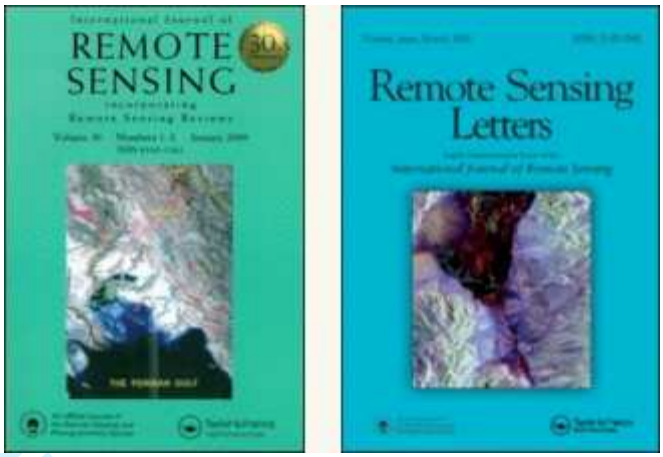


# Deriving an Inter-sensor Consistent Calibration for the AVHRR Solar Reflectance Data Record.

| | |
|---|---|
| Journal: | *International Journal of Remote Sensing* |
| Manuscript ID: | TRES-PAP-2009-0731.R1 |
| Manuscript Type: | IJRS Research Paper |
| Date Submitted by the Author: | 23-May-2010 |
| Complete List of Authors: | Heidinger, Andrew; NOAA/NESDIS, Center for Satellite Applications and Research<br>Straka III, William; University of Wisconsin, CIMSS<br>Molling, Christine; UW Madison, CIMSS/SSEC<br>Sullivan, Jerry; NOAA Science Center (WWB), (now retired)<br>Wu, Xiangqian; NOAA/NESDIS, Center for Satellite Applications and Research |
| Keywords: | AVHRR, CALIBRATION, CLOUDS, CLIMATOLOGY |
| Keywords (user defined): | |
| | |

# Deriving an Inter-sensor Consistent Calibration for the AVHRR Solar Reflectance Data Record.

**A. K. Heidinger*†, W. C. Straka III‡, C. C. Molling‡ , J. T. Sullivan§≠ and X. Wu§.**

†NOAA/NESDIS Center for Satellite Applications and Research, Madison, Wisconsin, USA

‡University of Wisconsin, Madison, Wisconsin

§ NOAA/NESDIS Center for Satellite Applications and Research

≠ now retired

*Correspondence to: A. K. Heidinger (Andrew.Heidinger@noaa.gov)



## Abstract

A new set of reflectance calibration coefficients has been derived for channels 1 (0.63 μm) and 2 (0.86 μm) of the Advanced Very High Resolution Radiometer (AVHRR) flown on the NOAA and EUMETSAT polar orbiting meteorological satellites. This paper uses several approaches that are radiometrically tied to the observations from NASA's MODIS imager to make the first consistent set of AVHRR reflectance calibration coefficients for every AVHRR that has ever flown. Our results indicate that the calibration coefficients presented here provided an accuracy of approximately 2% for channel 1 and 3% for channel 2 relative to that from the MODIS sensor.

## 1 Introduction

With the successful launch of NOAA-19 in February 2009, the National Oceanic and Atmospheric Administration (NOAA) has successfully launched the 13th and final satellite of the polar orbiting environmental satellites (POES) program. The imager on the POES series is the Advanced Very High Resolution Radiometer (AVHRR) whose primary mission was to provide cloud imagery and sea surface temperature estimates (Schwalb, 1982). However, AVHRR data was soon found capable of providing quantitative estimates of many critical atmospheric and surface parameters (Cracknell, 1997). With the presence of the AVHRR on the European Organisation for the Exploitation of Meteorological Satellites' (EUMETSAT) Metop program, AVHRR data record should continue until 2018 and therefore span over 40 years when finished.

With its long and continuous data record, the AVHRR has become a key contributor to our ability to estimate multi-decadal climate variability from satellites. Numerous studies have used AVHRR time-series to conduct multi-decadal climate studies (Wang and Key, 2003; Evan et al., 2006, Zhao et al, 2008). However, one of the main weaknesses of the AVHRR

* Corresponding author. Email: Andrew.Heidinger@noaa.gov, TEL: 608-263-6757, FAX: 608-262-5974

for climate studies is the uncertainty in the calibration of the solar reflectance channels due to the lack of any on-board calibration source. Typically the AVHRR reflectance channels are calibrated pre-launch by the instrument vendor. After launch, the responsiveness of the AVHRR decreases with time for reasons not fully understood and not predictable. In addition, the initial calibration directly after launch can also differ greatly from that determined during the pre-launch testing period. Therefore, the pre-launch reflectance calibration is often of little use for quantitative remote sensing applications. Several methods have been developed for estimating the post-launch calibration. Generally, most of the published literature has dealt with methods that calibrate the AVHRR reflectance channels by assuming the reflectance properties of particular regions of the earth. However, with the launch of advanced imagers, such as Moderate Resolution Imaging Spectroradiometer (MODIS) on the National Aeronautics and Space Administration's (NASA) Earth Observing System (EOS) platforms, well-calibrated imager data with spectral and spatial characteristics comparable to the AVHRR are available.

The goal of this paper is to provide the AVHRR remote sensing community with a set of calibration coefficients for all of the sensors derived from a consistent approach. This has never been done in the literature in a single paper using a single approach. While the approach laid out in the following sections involves use of Antarctic and desert targets and data from Simultaneous Nadir Overpasses (SNOs), each of these components is ultimately tied to the calibration of MODIS. A companion paper to this one (Molling et al., 2009) compares the result of the calibration developed here to other existing long-term AVHRR reflectance calibration methods. A specific goal of this paper is to provide documentation and error characterization of the solar reflectance calibration used in the AVHRR Pathfinder Atmospheres Extended (PATMOS-x) data set.

## 2 Statement of the Problem

As stated above, a companion paper (Molling et al., 2009) will compare the calibration results derived here against those from other available datasets. However, to motivate this work, a brief example of the state of the AVHRR reflectance calibration is warranted. Figure 1 shows a time-series of the nadir channel-1 and channel-2 reflectance during July over a Northern Greenland Target derived from two morning orbiting AVHRR sensors (NOAA-12 and NOAA-15). This target was chosen since the channel-1 and channel-2 reflectances should be constant over this period because both the surface reflectance and the solar illumination are nearly constant. The target spans from 73-78N and 45-35W and is subset of the Greenland Target used by Tahnk and Coakley (2001a). The reflectances where computed by averaging all pixels that fell within the target regardless of solar and sensor viewing geometries. During this month, the range in solar zenith angle was 53 to 69 and the range in sensor zenith angle was 7 to 57 degrees. The reflectances were derived from the same channel counts and differences in reflectance arise from differences in the calibration, not due to sampling differences. While treatment of specular effects would be required to make an accurate time-series of surface reflectance, this analysis is solely focused on the impact of the calibration. The vertical line represents the transition between NOAA-12 and NOAA-15. The PATMOS-x reflectance time-series is derived from the calibration methodology presented here. As described later, this methodology employs techniques that guarantee continuity in satellite-to-satellite transitions. In contrast, the ISCCP calibrations do not result in a continuous time series and differ significantly from the PATMOS-x values. It is important to note that the

ISCCP calibration is a well-accepted and well-used dataset especially when applied to the afternoon orbiting AVHRR sensors. Other well-known calibration sets have focused exclusively on the afternoon orbiting sensors and therefore cannot be plotted in Figure 1. The exclusion of the morning satellites by most of the previous calibration efforts is yet another motivating factor for this study. Also shown in Figure 1 is the reflectance time series provided by the prelaunch calibration data provided by NOAA's National Environmental Satellite Information Data and Information Service (NESDIS). Note that it clearly provides an inaccurate estimate of the reflectance and one that is not consistent between sensors. So in summary, the following reasons motivate this work: (1) The inaccuracy of the prelaunch calibration data. (2) The lack of temporal consistency in some of the existing calibration data sets. (3) The lack of consistent calibration data for all AVHRR sensors including those in the morning orbits. The calibration derived here will address all of these issues.

## 3 Terminology

The AVHRR solar reflectance calibration consists of two terms. The first term is the difference in the measured count, C, and the dark count, $D$. The dark count is what the instrument would measure under dark conditions. In this analysis, the values of $D$ are taken from those actually measured during the space views within the scan pattern of the AVHRR. The second term is the calibration slope, $S$, which is also known as the inverse-gain. The AVHRR calibration equation can be written as

$$R_{cal} = S(C - D) \tag{1}$$

where $R_{cal}$ is the value generated from the calibration and is referred to as a scaled radiance. $R_{cal}$ can be expressed as

$$R_{cal} = 100\,\pi I / \overline{F_o} \tag{2}$$

where $I$ is the radiance and $\overline{F_0}$ is the channel-averaged annual-mean solar exoatmospheric flux contained within the AVHRR channel's spectral response function. The units of $\overline{F_o}$ used in this work are W/m$^2$/cm$^{-1}$ and the units of $\boldsymbol{I}$ are W/m$^2$/cm$^{-1}$/str. $R_{cal}$ is dimensionless and is related to the true isotropic reflectance, $R$, used most often in remote sensing as

$$R = 100\,\pi I / \mu_o F_o = d^2\, R_{cal} / \mu_o \tag{3}$$

where $d^2$ is the sun-earth distance factor and $\mu_o$ is the cosine of the solar zenith angle. Note that Fo, the channel-averaged solar exoatmospheric flux, is defined as $F_o = \overline{F_o} / d^2$ and the scaled radiance and reflectance values are scaled to range from 0 to 100%.

Throughout this work, the count values, $C$, will refer to the 10-bit instrument counts that would be measured by a single gain instrument. Starting with the AVHRR/3 series, the channel-1, channel-2 and channel-3a observations were computed with a dual-gain calibration. This was done to increase the sensitivity of the observations to dark scenes for improved aerosol optical thickness estimates. In this analysis, we have converted the dual-

gain counts measured by the AVHRR/3 sensors back to what a single-gain count would have been. Appendix A discusses this conversion and demonstrates its accuracy.

The goal of this analysis is to use MODIS to determine values of $R_{cal}$ that can be used with appropriately observed values of $C$ and $D$ from AVHRR to derive a consistent time-series of $S$ for each AVHRR channel for all sensors.

This paper will be focused on Channel 1 (channel-1) and 2 (channel-2) of the AVHRR. Figure 2 shows the spectral response functions of a single AVHRR (NOAA-17) overlaid on top of a nadir transmission spectrum computed for the standard tropical atmosphere. The AVHRR/3 series also includes a channel at 1.6 μm (Channel 3a), which has been available intermittently since 1998. This paper will not deal with Channel 3a though future work will extend these techniques to this channel. Figure 2 clearly demonstrates that while channel-1 falls in a very transmissive region of the spectra, channel-2 encompasses the water vapour rotation bands at 0.82 and 0.94 μm. The channels on MODIS used to calibrate the AVHRR channels are shown in Figure 3. While the central wavenumbers of channel-1 and channel-2 on MODIS are similar to those on the AVHRR, the MODIS channels are narrower and channel-2 on MODIS is located to avoid any appreciable water vapour absorption. Another complicating issue is the variation in the spectral response function (SRF) from one AVHRR to the next. Table 1 provides the effective wavelength and integrated solar energy for the AVHRR channel-1 and channel-2 spectral response functions provided by the NOAA/NESDIS Center for Satellite Applications and Research (STAR) (http://www.star.nesdis.noaa.gov/smcd/spb/fwu/solar_cal/AVHRR.html). The methodology described later does account for the variation in the SRF for each AVHRR sensor.

## 4 Review of Past Work

The amount of literature surrounding techniques to calibrate the AVHRR solar reflectance channels is large and a proper summary is not possible here. The companion paper to this one, Molling et al. (2010), provides a brief summary of these past efforts. The vast number of successful climate studies in existence today is a testament to remarkable skill of these previous studies. The advent of satellite visible and near-infrared imagers with on-board solar calibration has ushered in a new period in AVHRR calibration because it has allowed for direct calibration of the AVHRR solar reflectance channels. Besides MODIS, the data from the Visible and Infrared Scanner (VIRS) and the Along Track Scanning Radiometer (ATSR) imagers have also been used for this purpose. While not applied to the AVHRR, Minnis et al. (2002), demonstrated the use of VIRS, MODIS and ATSR data to calibrate geostationary imagers. Heidinger et al. (2002) used MODIS to calibrate the AVHRR solar reflectance channels for NOAA-16, which was the first of the dual-gain AVHRR instruments in the traditional afternoon orbit. In addition to directly calibrating AVHRR, work has been done on using these advanced sensors to redefine the reference reflectance values of stable earth targets.

In summary, there is a long and evolving history of the methods available to calibrate the solar reflectance of the AVHRR. In general, the past works have employed approaches to one or a limited subset of the AVHRR sensors. The methodology employed here, described in the next section, builds upon these past works and attempts to apply a uniform methodology to the entire AVHRR data-record.

## 5 Methodology

The goal of this study was to use the MODIS record to recalibrate AVHRR solar reflectance channels so that they provide an accurate and temporally consistent basis for climate data records that rely on solar reflectance observations. During the MODIS era (2000-2009+), this can be accomplished through direct comparison of MODIS and AVHRR observations taken during appropriate times of coincidence. However, for data prior to the MODIS era, we use assumed radiometrically stable earth scenes as reference values after they have been characterized by MODIS. As discussed below, we have chosen the traditional Libyan Desert Target (Rao and Chen, 1995; Yu and Wu, 2009) and a Committee of Earth Observations from Satellites (CEOS) recently endorsed target located over Dome C in Antarctica. While the number of potential choices is endless, we feel that inclusion of these two drastically different but stable references is adequate. In addition to above methods to recalibrate AVHRR from MODIS, we can also compare AVHRR sensors together when more than one is in operation as is the case for most of the record. These AVHRR to AVHRR comparisons provide a means to assess the inter-satellite consistency. Therefore this methodology is based on four absolute sources of calibration data, all of which are tied to MODIS. The remainder of this section provides a more detailed discussion of each of these methods.

### 5.1 Conversion of MODIS Reflectances to AVHRR Reflectances

Beyond the processing of the satellite observations over the target areas and over regions consisting of SNO occurrences, a major part of this effort involves converting the MODIS observations into what a perfectly calibrated AVHRR sensor would observe in order to derive the AVHRR calibration slopes. Runs of the MODTRAN4 radiative transfer code (Anderson et al., 1999) provide the basis for this conversion. The methods used to do this conversion vary in the details for the MODIS SNO, DOME-C and LIBYA methods and these details are discussed in the remainder of this section. For all methods, MODTRAN4 was run using the TIGR3 (TOVS Initial Guess Retrieval Version 3) atmospheric profile database provided by the Laboratoire de Météorologie Dynamique (LMD). The surface reflectance data came from various surface reflectance spectra provided as options in the MODTRAN4 model.

The conversion of the MODIS to AVHRR reflectances for the MODIS/AVHRR SNO events is done according to the methodology laid out by Heidinger et al. (2002). In this work, the ratio of the AVHRR to MODIS reflectances was shown to be well correlated with the ratio of the MODIS Channel 18 to Channel 17 reflectances. MODIS Channel 18 and 17 are located in the 0.94 mm water vapour band. This ratio therefore is itself correlated with the total path water vapour encountered by the photons that comprise the observed reflectance. This is critical because the MODIS/AVHRR SNO data includes cloudy observations so that knowledge of the clear-sky total precipitable water (TPW) does not guarantee the ability to accurately convert MODIS to AVHRR reflectances. However, using the MODIS Ch18 to Ch17 ratio automatically accounts for the effect of clouds of various heights. MODTRAN4 was run using all of the TIGR3 profiles above 60° N. The surface reflectance was taken from the MOSART Sea Ice model provided in MODTRAN. When layers were determined to be saturated, clouds were placed within them. The standard MODTRAN4 cloud models were employed to simulate cloudy atmospheres. A water cloud model was employed for clouds with heights less than 4 km and an ice cloud model was employed for clouds with heights greater than 4km. A marine aerosol profile was assumed. MODTRAN4 was run to simulate

nadir reflectances from AVHRR and MODIS for randomly varied solar zenith angles and randomly selected profiles within the defined region. This computation was done for each AVHRR sensor that witnessed an SNO event with a MODIS sensor. The regression is the same as that in Heidinger et al. (2002) and is given below.

$$R_{avhrr}/R_{\mathrm{mod}\ is} = a_{sno} + b_{sno}\left(R_{18}/R_{17}\right) + c_{sno}\left(R_{18}/R_{17}\right)^2 \quad (4)$$

Table 2 and Table 3 give the coefficients ($a_{sno}$, $b_{sno}$ and $c_{sno}$) computed using the methodology described above.

Unlike the MODIS/AVHRR SNO events where the MODIS Ch18 and Ch17 ratios can be used to predict the AVHRR values, the DOME-C and LIBYA AVHRR observations occur without simultaneous MODIS observations. Therefore the method applied during the MODIS/AVHRR SNO won't work for the DOME-C and LIBYA methods. For these methods, the basis of the conversion is the TPW information provided by the NCEP reanalysis. Unlike the MODIS/AVHRR SNO method, this is possible because the DOME-C and LIBYA methods involve only clear-sky measurements. To generate the regressions to perform the TPW-based regressions, MODTRAN4 was run to simulate the AVHRR and MODIS nadir clear-sky reflectances. For LIBYA, only TIGR3 profiles over the Saharan Desert were used. For DOME-C, only TIGR3 profiles from latitudes poleward of 66°S were used. The surface reflectance spectrum for LIBYA was modelled using the MOSART Desert spectrum and the surface reflectance spectrum for DOME-C was modelled using the MOSART Antarctic Snow spectrum. For LIBYA, the default desert aerosol model is used and the maritime model is used for DOME-C. The specific form of the regression used for the LIBYA and DOME-C conversion is shown below.

$$R_{avhrr}/R_{\mathrm{mod}\ is} = a_{libya} + b_{libya}\left(\ln(tpw)\right) + c_{libya}\left(\ln(tpw)\right)^2 + d_{libya}\left(\ln(tpw)\right)^3 \quad (5)$$

This regression is applied to both channel-1 and channel-2. In (5), $tpw$ refers to the total path water, where the path is defined by the sun-surface-sensor geometry. A more accurate regression was found using $\ln(tpw)$ as opposed to $tpw$. Table 4 and Table 5 provide the channel-1 and channel-2 regression coefficients $a$, $b$ and $c$ for LIBYA and

Table **6** and

Table 7 provide the same information for DOME-C.

## 5.2 MODIS to AVHRR SNOs

As demonstrated by Heidinger et al. (2002), observations from MODIS and AVHRR during periods of a Simultaneous Nadir Overpass (SNO) can be used to accurately transfer the MODIS reflectance calibration to AVHRR. The SNO occurrences happen multiple times per month with each occurrence providing a large number of observations. To maximize the dynamic range, we limited the SNO data analyzed here to be between June and August of each year and to occur in the Northern Hemisphere (typically above the Arctic Circle). A typical SNO scene therefore includes open water, cloud and sea ice. Observations over land were ignored to avoid the uncertainty associated with the large spectral variation in vegetation reflectances.

The conversion of the MODIS reflectances into AVHRR reflectances was accomplished using the method described above. Before being used in the SNO calculations, the MODIS and AVHRR observations were mapped to a 0.50° equal-area grid. This was done to avoid the costly renavigation required to achieve agreement using pixel-level results shown by Heidinger et al. (2002). The SNO observations consisted of the mean values of the MODIS channel-1 and channel-2 reflectances and of the AVHRR channel-1 and channel-2 counts. Only grid-cells where the mean sensor zenith angle was less than 5° and the MODIS-AVHRR time differences were within 5 minutes were used. Figure 4 shows an example of the SNO observations for July 2007 for channel-1 for NOAA-18 AVHRR and AQUA/MODIS. The calibration slope for each month of SNO's was computed by forcing the linear fit through the origin of the MODIS reflectances as a function of the AVHRR counts. To avoid the impact of outliers at low values of reflectance, only grid-cells with mean count values greater than 100 are used in the slope calculation. To date, we have performed the SNO analysis for all July SNO occurrences between NOAA-14, 15, 16, 17, 18, 19 and Metop-A and MODIS (AQUA and TERRA).

## 5.3 Dome C

While the MODIS SNO analysis provides the best direct calibration source of the four used here, it is obviously only available during the MODIS era (2000-2009+) which is only one third of the AVHRR era. Our chosen method of extending the MODIS reference back in time is to use MODIS to characterize stable earth targets and use these reference values during the entire AVHRR era. During the MODIS era, we can compare the calibration results from the earth targets to those from the MODIS/AVHRR SNO analysis and ensure that results are consistent.

One obvious choice for stable earth targets are the polar ice sheets. Use of targets on the Greenland Ice Sheet for calibration studies was demonstrated by Loeb (1997). Recently, the Committee of Earth Observations from Satellites has endorsed and promoted several earth targets to serve as calibration targets. One of these endorsed sites is the Dome C region in Antarctica (75°S, 123°E). Dome C provides a stable, dry and clear atmosphere that has proven ideal for astronomical observations. These same conditions also make it ideal as an earth reference target for satellite calibration studies because it lessens the uncertainties

associated with the water vapor corrections and cloud clearing. Another major advantage of Dome C or any polar target is that it is viewed during daylight conditions by AVHRR sensors in any orbit during the summer months. This is not the case for the typical desert targets that occur in the sub-tropics.

To determine the reference values for Dome C, values of the mean nadir channel-1 and channel-2 MODIS reflectances over the target were computed for the months of December, January and February for TERRA and AQUA from 2000 to 2008. Figure 5 shows the variation in the MODIS channel-1 reflectances plotted against the solar zenith angle in a manner similar to Cao et al. (2008). The benefits of regressing the reflectance times the cosine of solar zenith angle versus the solar zenith angle are that the variation is nearly linear. Note that solar zenith range provided by the MODIS is roughly 58 to 80˚. Therefore, only nadir AVHRR observations that fall within this range can be calibrated using the MODIS Dome C data.

To generate the DOME-C calibration slopes, the procedure is as follows. The mean single-gain AVHRR counts and dark-counts for channel-1 and channel-2 are computed over the Dome C target. The corresponding mean solar zenith angle is used in conjunction with regression in Figure 5 to provide the MODIS reflectance value (what MODIS would have observed at that sun-angle). The TPW from the NCEP Reanalysis for that time over Dome C is used with the regression in Table 4 to compute the conversion from the MODIS reflectance to the AVHRR reflectance. Equation (1) is used to estimate the calibration slope, which is then typically averaged with all calibration slopes computed from DOME-C for a particular AVHRR channel for one month. These monthly averaged values are then used in the final calibration slope time series estimates.

For this analysis, the AVHRR and MODIS data were composited over 0.50° equal-area grid-cells. For DOME-C, detection of cloud is challenging. For this analysis, cells were excluded if the standard deviation of the 11 μm brightness temperature exceeded a threshold of 0.2 K or if the standard deviation of the 0.63 μm reflectance exceed a threshold of 0.2%. DOME-C observations were also excluded when the solar zenith angle exceed 75˚. The thresholds were determined by manual analysis. However, the occurrence of cloud over Dome C is rare which contributes to its popularity with the astronomical community. Only days when all DOME-C grid-cells were deemed cloud-free were included in the analysis. This screening results in an exclusion of 26 % of the data. The data from these clear days were used in the procedure described above to generate a calibration slope for channel-1 and channel-2.

### 5.4 Libyan Desert

While Dome C offers an excellent earth calibration target, it only provides data during those parts of the year where Antarctica is sunlit. In contrast, non-polar targets are sunlit for parts of every day throughout the year and provide a method for continuous monitoring of the variation of the reflectance calibration. However, because no MODIS sensor views these non-polar targets at the large solar zenith angles characteristic of the AVHRR sensors in the

morning orbits, mid-latitude sites can not be used to calibrate morning orbiting sensors with out the increased uncertainties associated with extrapolation.

The Libyan Desert Target (LDT, 21-23°N, 28-29°E) used in this study is the one used in the studies by Rao and Chen (1995). The LDT was first recommended for use as a calibration site by Staylor (1990) and calibration results derived from it were found to be consistent with those from other desert sites (Heidinger et al., 2002). Even though this site is dry in a relative humidity sense, the warm temperatures do allow for the presence of significant values of TPW that result in significant differential water vapour absorption between the MODIS and AVHRR channel-2.

A nearly identical process was used to generate the reference reflectance for the LDT as the DOME-C target. The only difference was that the NESDIS operational cloud mask (available in the level-1b data) was used in the cloud-clearing process. As was the case with DOME-C, LDT data for a given day were used only if all of the grid-cells that comprised the LDT were determined to be totally clear. Figure 6 shows the resulting nadir MODIS channel-1 and channel-2 reflectance values for the LDT as a function of solar zenith angle plotted in a similar manner to that used in Figure 5. The computation of the calibration slopes follows the same process outlined for DOME-C above. Values were generated for each month where the AVHRR viewed the LDT within the solar zenith angle provided by MODIS. As the afternoon AVHRR orbits drifted to later equator crossing times, use of the MODIS-derived LDT reference values to estimate calibration slopes was discontinued.

### 5.5 AVHRR to AVHRR SNO's

The fourth and last method of determining calibration slopes is provided by the analysis of SNO occurrences between two AVHRR sensors. Throughout most of the period since the launch of NOAA-6 in 1980, NOAA has flown two POES spacecraft with one in a morning and one in an afternoon orbit. Data gaps in the NOAA-6 and NOAA-8 GAC archives in CLASS have limited the number of AVHRR to AVHRR SNO values before the launch of NOAA-10 in 1986. However after 1986, the CLASS archive allows for an almost complete record of July SNO observations from all AVHRR sensors.

An example AVHRR to AVHRR SNO analysis for July 1993 from NOAA-11 and NOAA-12 is shown in Figure 7. The count values for the AVHRR/3 sensors are the equivalent single gain counts discussed in Appendix A. The slope provided by a linear regression of the relative count values (counts minus dark counts) of one AVHRR to another provides the ratio of the calibration slopes of one AVHRR to another. As was done with the AVHRR to MODIS analysis, the linear regressions were forced to go through the origin. Table 4 provides the slope ratios and the R2 values of the linear regressions for all of the SNO computed in this analysis.

The AVHRR to AVHRR SNO values provide no direct absolute values of the calibration slopes. They do provide a means of transferring the results of the other methods that do provide direct absolute values of calibration slopes to other sensors. For example, though morning satellites never see the LDT within the acceptable solar zenith angle range to apply the MODIS reference values, the AVHRR to AVHRR SNO values allow LDT results from the afternoon satellites to estimate the calibration slopes of the morning satellites. In addition, the DOME-C results for morning satellites can be used to estimate the slopes of the afternoon satellites. As discussed in the next section, the information supplied by the AVHRR to

AVHRR SNO's provides a critical test of the consistency of the AVHRR reflectance climate records.

## 6 Determination of Calibration Slope Time Series

The previous sections described the methods used to generate the channel-1 and channel-2 calibration slopes throughout the lifetime of the various sensors. In this section, the independent estimates of calibration slopes are combined to derive a final expression to predict the calibration slopes as a function of time. To compute the final time series, the estimated calibration slopes from the four methods described above are used in a least-squares fitting method (Sullivan, 1980).

Our experience with the AVHRR indicates that a second order polynomial is a good model for the calibration slope time series. For this analysis, the specific form of the slope time series, $S(t)$ is given by the following expression

$$S(t) = S_0\left(100 + S_1 * t + S_2 * t^2\right)/100. \quad (6)$$

Where $S_0$ is the calibration slope at time=0 and $t$ is the time after launch expressed in years.

### 6.1 Error Estimates

Proper application of any fitting technique demands appropriate weighting of the data points. Given the very different assumptions employed by the methods described above, an assumption that the errors associated with each technique are the same is not valid. The error estimates of each technique have three main components. The first is the overall accuracy of the MODIS values themselves. The second is the accuracy of the spectral conversion of the MODIS values to the AVHRR values. And the last main component is the assumption of radiometric stability over time. The next paragraphs will argue for the error estimates used for each calibration source.

The stated accuracy of the MODIS reflectances is 2% (Xiong et al., 2005) and this uncertainty will be assumed for all of the MODIS data used in this analysis. The major error in the spectral conversion from MODIS to AVHRR is in the uncertainty in the water vapour profiles. For the MODIS to AVHRR SNO analysis, this error is assumed negligible since they occur in the relatively dry Arctic conditions and the MODIS near-infrared channels are used to estimate the water vapour effects directly. And because of the strict SNO criteria, it is argued that temporal stability errors are also negligible. Therefore, the errors assumed for the AVHRR/MODIS SNO slope values are 2%. Since all of the calibrations are ultimately tied to MODIS, the assumed error of the MODIS observations has little relative impact on the results presented here.

For DOME-C, the errors due to water vapour uncertainty are also negligible due its Antarctic environs. Also, there appears to be no known reason to expect changes in its surface reflectance over the past thirty years. The work of Warren (1982) and Hudson et al. (2006) demonstrate that snow reflectance spectra can vary with snow-grain properties. The ASTER spectral library provides reflectance spectra for snow surfaces with fine, medium and coarse-grained snow. If all three spectra are used to compute the conversion factor from MODIS to

AVHRR, the difference does not change by more than 1% for either channel. Therefore, we assign a 1% error to surface reflectance component of the MODIS to AVHRR conversion. The total uncertainty assumed for the DOME-C results is 3% for both channels, which includes the assumed uncertainty in the MODIS calibration.

Unlike DOME-C, the LDT does have a non-negligible amount of water vapour. The TPW values over the LDT range from about 1 cm during the winter to about 2 cm in the summer. Assuming an annual mean TPW value of 1.5cm, the slope of the channel-2 transmission with TPW is -0.062 / cm based on the regression shown in Table 5. Assuming the NCEP reanalysis estimates of TPW have an uncertainty of 30% (Bony et al., 1997), the uncertainty in the channel-2 transmission is roughly 1.5%. For channel 1, water vapour uncertainty impacts should be negligible. The surface reflectance component is more problematic. We assume a 2% uncertainty is a conservative estimate. Therefore, the LDT analysis is assumed to have an uncertainty of 2% for channel-1 and 3.5% for channel-2 on top of the 2% assumed for the MODIS observations.

### 6.2 Calibration Slope Fit Results

Examples of the resulting time series of calibration slopes are given in Figure 8 through Figure 10. Figure 8 shows the results for NOAA-18, which resides entirely in the EOS era and therefore has data from all the calibration sources discussed above. The solid circles provide the values of the calibration slopes derived from the MODIS/AVHRR SNO's. The plus symbols give the slopes from the Libya Desert Target and the triangle symbols give the slopes from the Dome-C Target. The light grey symbols give the slopes derived from transferring those of other AVHRR's via AVHRR/AVHRR SNO events. The plot on the left is for channel-1 and the plot on the right is for channel-2. Given in the bottom legend of Figure 8 are the coefficients of a quadratic fit of the calibration slope over time expressed as years since launch. Also in the bottom legend, are the bias and standard deviations of the fit with respect to all of the data. Note that the bias of the fit is not zero because of the varying weights assigned to the different calibration sources. The bias and standard deviation numbers are computed as percentages of the mean value. Given in the legend on the top left corner of each plot are the bias and standard deviation. A discussion of these bias and standard deviations is given later.

Figure 9 shows the analogous version of Figure 8 for NOAA-7. NOAA-7 occurred solely in the pre-EOS era and due to holes in the AVHRR GAC archive, saw no AVHRR/AVHRR SNO values. Therefore, the NOAA-7 calibration curve derives solely from the Libyan Desert and Dome C Targets. Figure 10 shows the calibration curve for NOAA-14. This satellite provided data before and after the EOS era. After 2000, MODIS/AVHRR SNO data from Terra/MODIS are available. One important feature of Figure 10 is continuity of the post- and pre-EOS calibration sources. A summary of all calibration slope fits is in Table 8.

Figures 10 through 13 provide the bias and standard deviation plots for both channels for all of the satellites and all of the calibration sources. The x-axis in these figures is the satellite number with 2 referring to METOP-A and 5 referring to TIROS-N. As stated above, these numbers are computed as percentage values relative to the mean value. Figure 11 shows the bias values for channel-1. Figure 11 shows the bias for final fits (ALL) are much less than

1% for all satellites. The bias values for the individual sources are higher and approach 2% for some sources on some satellites. It is important to note that fitting performs better for the earlier satellites that have less calibration data. If only one source of calibration data were available, the bias would be necessarily zero. There are some patterns of the biases in Figure 11. For example, the LDT biases are always negative except for the early morning satellites (NOAA-5,6,8,19,12). The Dome C biases are almost always positive for the afternoon and mid-morning satellites. Overall, no one ALL bias measurement exceeds 1% in magnitude.

Figure 12 shows the standard deviation of the different calibration slopes with respect to the derived calibration curves. The range of values when considering all points (ALL) is roughly 1% to 2.5% and when considering the individual sources the range is roughly 0.5% to 3%. In general, there is less satellite-to-satellite variation in the standard deviation than the bias. The small standard deviation associated with NOAA-6 is due to the small number of calibration points. Overall, Figure 11 and Figure 12 indicate that a representative bias and standard deviation for the AVHRR calibration of channel 1 is 0.5% and 2%. Using a simplistic root-mean-square calculation gives a total uncertainty for the AVHRR calibration of roughly 2%.

Figure 13 and Figure 14 show the channel-2 satellite to satellite variation of the bias and standard deviation of the derived calibration curves against the calibration sources. Figure 13 shows that the biases for the individual calibration sources differ from those for channel-1. Notably, the MODIS/SNO values tend to have a negative bias while the other calibration sources give positive biases in the EOS era. One explanation for this discrepancy is an inconsistency in the water vapour corrections derived during the MODIS/SNO events and the corrections derived form the LDT and Dome C, which are based on the NCEP-Reanalysis data. Given that the water vapour corrections often modify the slopes by 10 to 20%, a residual error of 1-2% is expected. The very large negative bias for the MODIS/SNO data for NOAA-14 is exaggerated by the fact that there are only two MODIS/SNO data points (TERRA 2000 and 2001). In addition, the standard deviations for channel-2 are also higher by 0.5% than the values seen in Figure 12 for channel-1. Overall, Figure 13 and Figure 14 indicate that a representative bias and standard deviation of the AVHRR calibration of channel-2 is 1% and 2.5%. Therefore a total uncertainty of the AVHRR channel-2 calibration is roughly 3%.

## 7 Conclusions

This study has combined very different approaches together to estimate the channel-1 and channel-2 calibration slopes for every AVHRR. While each calibration source offered different surface, atmospheric and sun angle viewing characteristics, the methods employed here generated consistent results. We argue that this consistency will allow for generation of climate records from the AVHRR that result in time-series that do not suffer from sensor-to-sensor calibrations differences that exceed those quoted here. It is worth repeating that all of the calibration slopes and their uncertainties given here are relative to MODIS. Any systematic errors in MODIS would not be corrected in this analysis. Our results indicate that we successfully transferred the MODIS calibration to AVHRR with an approximate accuracy of 2% for channel-1 and 3% for channel-2. While calibration slopes estimates for NOAA-6

and 8 are provided, the dearth of data makes an estimate of their error more challenging and caution should applied in their use.

In the future, we plan to work with other AVHRR data owners and try to fill in the gaps in NOAA CLASS AVHRR GAC archive so that more data points can be obtained for TIROS-N, NOAA-6, and NOAA-8. In addition, a relaxation of the reliance on the accuracy of MODIS can be obtained if data from other sensors with onboard reflectance calibration such as Visible and Infrared Scanner (VIRS) and Advanced Along-Track Scanning Radiometer (AATSR) are used. The MODIS/AVHRR SNO observations are also being reanalyzed to develop new reflectance calibration parameters for channel-3a. In the future, we intend to apply this methodology to future AVHRR sensors including Metop-B&C. We expect that improvements in our knowledge of the surface reflectance over surface targets and our ability to correct for atmospheric effects will lead to future studies with improved accuracy.



## Appendix A: Conversion of Dual-Gain Counts

For AVHRR/1 and AVHRR/2, all channels were calibrated using a single gain calibration slope. Starting with the AVHRR/3 series, the solar reflectance bands (channel-1, channel-2 and ch3a) on the AVHRR were calibrated using a dual-gain calibration slope. The AVHRR counts (dual or single gain) range from a dark count of about 40 to the maximum value allowed by a 10 bit system of 1023. For the single-gain channels, a scaled radiance ($R_{cal}$) of 50% occurs at a count value of approximately 500. For the AVHRR/3 series, a scaled radiance of 50% occurred for count value of approximately 250 for channel-1 and channel-2 and for a count value of 125 for ch3a. For the AVHRR/3 series, this was accomplished using an electronic gain setting. Based on casual communication with ITT engineers, the dual gain operation was accomplished for channel-1 and channel-2 by decreasing the calibration slope by 50% in the low end and increasing it by 150% in the end with the low/high switch or break-point occurring at dual-gain switch count, $B_{dg}$. The value of $B_{dg}$ was approximately 500 though specific values used in this analysis were those determined during the electronics calibration and quoted in the ITT instrument calibration handbooks for each sensor. With this assumption, one can express a single-gain count (C) in the low-count region in terms of the dual-gain counts ($C_{dg}$) using the formulation given in (A1) and one can express a single gain count (C) in the high-count region using the formulation given in (A2).

$$C = C_d + 0.5\left(C_{dg} - D\right) \text{ for } C_{dg} < B_{dg} \tag{A1}$$

$$C = B_{sg} + 1.5\left(C_{dg} - B_{dg}\right) \text{ for } C_{dg} > B_{dg} \tag{A2}$$

The single gain of the switch count ($B_{sg}$) is determined using $C_{dg} = B_{dg}$ in (A1). A similar procedure could be applied to channel 3a though this is not done here.

The verification of the dual to single gain count conversion comes from an inspection of the AVHRR/3 to MODIS and AVHRR/2 to AVHRR/3 SNO figures (i.e. Figure 4). The complete catalogue of SNO figures is available at http://cimss.ssec.wisc.edu/clavr/calibration. These figures show the AVHRR/3 single-gain counts plotted against a true single-gain instrument (either MODIS or AVHRR/2). If the above transformation were incorrect, the results would not be a straight line and kink would be apparent near the value of $B_{sg}$ (approximately 250). For all SNO figures generated for this analysis, no such kink is seen. Therefore, we argue the conversion to single-gain counts is valid and once this conversion is made, computed AVHRR/3 calibration slopes are valid for the entire AVHRR/3 count range.

## Acknowledgements

This study was funded in part by NOAA grant NA07OAR4310199. The views, opinions, and findings contained in this report are those of the author(s) and should not be construed as an official National Oceanic and Atmospheric Administration or U.S. Government position, policy, or decision.

## References

ANDERSON, G. P., BERK, A., ACHARYA, P. K., MATTEW, M. W., BERNSTEIN, L. S., CHETWYND, J. H. Jr., DOTHE, H., ADLER-GOLDEN, S., 1999, MODTRAN4: radiative transfer modelling for remote sensing., Proc. SPIE, Vol. 3866, doi:10.1117/12.371318.

BONY, S., SUD, Y., LAU, K.M., SUSSKIND, J. and SAHA, S., 1997, Comparison and Satellite Assessment of NASA/DAO and NCEP–NCAR Reanalyses over Tropical Ocean: Atmospheric Hydrology and Radiation. *Journal of Climate*, **10**, pp. 1441–1462.

CRACKNELL, A.P., 1997, *The Advanced Very High Resolution Radiometer (AVHRR)* (Philadelphia: Taylor and Francis).

EVAN, A.T., HEIDINGER, A.K. and KNIPPERTZ, P., 2006, Analysis of winter dust activity off the coast of West Africa using a new 24-year over-water advanced very high resolution radiometer satellite dust climatology. *Journal of Geophysical Research*, **111**, Doi:10.1029/2005JD006336.

HEIDINGER, A.K., CAO, C. and SULLIVAN, J.T., 2002, Using Moderate Resolution Imaging Spectrometer (MODIS) to calibrate advanced very high resolution radiometer reflectance channels. *Journal of Geophysical Research*, **107**, Doi:10.1029/2001JD002035.

HEIDINGER, A.K., SULLIVAN, J.T. and RAO, C.R.N., 2003, Calibration of visible and near-infrared channels of the NOAA-12 AVHRR using time series of observations over deserts. *International Journal of Remote Sensing*, **24**, pp. 3635-3649.

HUDSON, S.R., WARREN, S.G., BRANDT, R.E., GRENFEL, T.C. and SIX, D., 2006, Spectral bidirectional reflectance of Antaric snow: Measurements and parameterization. Journal Geophysical Research – Atmospheres, **111**, doi:10.1029/2006JD007290

LOEB, N.G., 1997, In-flight calibration of NOAA AVHRR visible and near-IR bands over Greenland and Antarctica. *International Journal of Remote Sensing*, **18**, pp. 477-490.

McCLATCHEY, R.A., R.W. FENN, J.E.A. SELBY, F.E. VOLZ, and J.S. GARING, Optical properties of the atmosphere, ARCRL-71-0279, Air Force Geophysics Lab, Bedford, MA, 1971

MINNIS, P., NGUYEN, L., DOELLING, D.R., YOUNG, D.F., MILLER, W.F. and KRATZ, D.P., 2002, Rapid calibration of operational and research meteorological satellite imagers, Part I: Evaluation of research satellite visible channels as references. *Journal of Atmospheric and Oceanic Technology*, **19**, pp. 1233-1249.

MOLLING, C.C., HEIDINGER, A.K., STRAKA III, W.C. and WU, X., 2009, Calibrations for AVHRR channels 1 and 2: review and path toward consensus. *International Journal of Remote Sensing* (companion paper).

RAO, C.R.N. and CHEN, J., 1995, Inter-satellite calibration linkages for the visible and near-infrared channels of the advanced very high resolution radiometer on the NOAA 7, 9, and 11 spacecraft. *International Journal of Remote Sensing*, **16**, pp. 1931-1942.

SCHWALB, A., 1982, Modified version of the TIROS N/NOAA A-G Satellite Series (NOAA E-J) - Advanced TIROS N (ATN). NOAA Technical Memorandum NESS 116, (Washington, D.C.: NOAA).

STAYLOR, F.W., 1990, Degradation rates of the AVHRR visible channel for the NOAA 6, 7, and 9 spacecraft. *Journal of Atmospheric and Oceanic Technology*, **7**, pp. 411-423.

SULLIVAN, J.T., 1980, Accurate least-squares techniques using the orthogonal function approach. NOAA Technical Report, EDIS 33, 104p.

TAHNK, W.R. and COAKLEY, Jr., J.A., 2001a, Improved calibration coefficients for NOAA-14 AVHRR visible and near-IR channels. *International Journal of Remote Sensing*, **22**, pp. 1269-1283.

TAHNK, W.R. and COAKLEY, Jr., J.A., 2001b, Updated calibration coefficients for NOAA-14 AVHRR channels 1 and 2. *International Journal of Remote Sensing*, **22**, pp. 3053-3057.

TAHNK, W.R. and COAKLEY, Jr., J.A., 2002, Improved calibration coefficients for NOAA-12 and NOAA-15 AVHRR visible and near-IR channels. *Journal of Atmospheric and Oceanic Technology,* **19**, pp. 1826-1833.

VERMOTE, E. and KAUFMAN, Y.J., 1995, Absolute calibration of AVHRR visible and near-infrared channels using ocean and cloud views. *International Journal of Remote Sensing*, **16**, pp. 2317-2340.

WANG, X. and KEY, J.R., 2003, Recent trends in Arctic surface, cloud, and radiation properties from space. *Science*, **299**, pp.1725-1728.

WARREN, S. G., 1982, Optical Properties of Snow. Review of Geophysics and Space Physics, **20**, p. 67089.

XIONG, X.X., Che, N.Z. and Barnes W., 2005, MODIS on-orbit spatial characterization and performance. *IEEE Transactions on Geoscience and Remote Sensing*, **43**, pp. 355-365.

YU, F. and WU, X., 2009, Removal of contaminated pixels from the desert target for AVHRR vicarious calibration. *Journal of Atmospheric and Oceanic Technology*, 26, pp 1354-1366.

ZHAO, T.X.-P., LASZLO, I., GUO, W., HEIDINGER, A., CAO, C., JELENAK, A., TARPLEY, D. and SULLIVAN, J., 2008, Study of long-term trend in aerosol optical thickness observed from operational AVHRR satellite instrument. *Journal of Geophysical Research*, **113**, Doi:10.1029/2007JD009061.

**Table 1. Spectral Comparison of Channel-1 and -2 in AVHRR**

| Satellite | Channel-1 | | Channel-2 | |
|---|---|---|---|---|
| | Effective wavelength (μm) | Solar Flux ($Wm^{-2}$) | Effective wavelength (μm) | Solar Flux ($Wm^{-2}$) |
| TIROS-N | 0.700 | 443.7 | 0.840 | 308.3 |
| NOAA-6 | 0.632 | 177.7 | 0.832 | 229.6 |
| NOAA-7 | 0.630 | 175.1 | 0.839 | 256.8 |
| NOAA-8 | 0.638 | 180.5 | 0.829 | 238.1 |
| NOAA-9 | 0.634 | 188.5 | 0.833 | 247.2 |
| NOAA-10 | 0.628 | 175.7 | 0.836 | 227.2 |
| NOAA-11 | 0.635 | 181.4 | 0.832 | 236.9 |
| NOAA-12 | 0.638 | 197.6 | 0.832 | 225.9 |
| NOAA-14 | 0.639 | 203.5 | 0.841 | 246.2 |
| NOAA-15 | 0.633 | 138.0 | 0.840 | 236.6 |
| NOAA-16 | 0.632 | 132.0 | 0.842 | 237.9 |
| NOAA-17 | 0.634 | 140.5 | 0.843 | 245.1 |
| NOAA-18 | 0.635 | 130.62 | 0.847 | 250.1 |
| NOAA-19 | 0.636 | 126.77 | 0.832 | 225.70 |
| Metop-A | 0.633 | 137.4 | 0.843 | 231.6 |

**Table 2. Regression coefficients for the conversion of AVHRR to MODIS Channel-1 using MODIS Ch18/Ch17.**

| Satellite | a | b | c |
|---|---|---|---|
| NOAA-14 | 1.00513 | -0.102997 | 0.110895 |
| NOAA-15 | 1.00645 | -0.00737838 | 0.00266143 |
| NOAA-16 | 1.01837 | -0.0537801 | 0.0383947 |
| NOAA-17 | 1.01985 | -0.0410405 | 0.0285677 |
| NOAA-18 | 1.01992 | -0.0345878 | 0.0214772 |
| NOAA-19 | 1.00471 | -0.00696835 | 0.00142683 |
| Metop-A | 1.00048 | -0.00322487 | 0.00235829 |

**Table 3. Same as Table 2 except for Channel-2.**

| Satellite | a | b | c |
|---|---|---|---|
| NOAA-14 | 0.713261 | 0.433532 | -0.166615 |
| NOAA-15 | 0.712781 | 0.409619 | -0.140453 |
| NOAA-16 | 0.715032 | 0.384575 | -0.116829 |
| NOAA-17 | 0.717761 | 0.392819 | -0.128791 |
| NOAA-18 | 0.696431 | 0.432846 | -0.153842 |
| NOAA-19 | 0.750041 | 0.338271 | -0.108837 |
| Metop-A | 0.720467 | 0.397555 | -0.136550 |

**Table 4. Coefficients for the conversion of MODIS to AVHRR Channel-1 Reflectances for the Libyan Desert Target**

| Satellite | a | b | c | d |
|---|---|---|---|---|
| TIROS-N | 1.00599 | -0.0114423 | -0.00183273 | -0.000364043 |
| NOAA-6 | 0.978124 | -0.00297255 | 0.000834962 | -0.000154794 |
| NOAA-7 | 0.977919 | -0.000175201 | -0.000120636 | 7.43374e-05 |
| NOAA-8 | 0.982983 | -0.00356397 | 0.000299373 | -5.81371e-05 |
| NOAA-9 | 0.976360 | -0.00267903 | 0.000883187 | -0.000313862 |
| NOAA-10 | 0.980072 | -0.000545169 | 0.000209821 | 3.71259e-05 |
| NOAA-11 | 0.976091 | -0.00110184 | -0.000255403 | -6.14536e-05 |
| NOAA-12 | 0.984771 | -0.00293191 | 0.000435105 | -0.000208083 |
| NOAA-14 | 0.989633 | -0.00206487 | -0.000407858 | -0.000124238 |
| NOAA-15 | 0.988021 | -8.94897e-05 | 0.000196634 | 2.75034e-05 |
| NOAA-16 | 0.985345 | -0.000151386 | 3.53531e-05 | 4.68175e-05 |
| NOAA-17 | 0.993283 | 0.000236726 | 8.73595e-05 | 0.000115394 |
| NOAA-18 | 0.994808 | 4.24846e-05 | 0.000262774 | 8.67677e-05 |
| NOAA-19 | 0.989766 | 0.000142673 | 8.67653e-05 | 0.000103419 |
| Metop-A | 0.985385 | 0.000216014 | -2.47965e-05 | 9.18556e-05 |

**Table 5. Same as Table 2 for Channel-2**

| Satellite | a | b | c | d |
|---|---|---|---|---|
| TIROS-N | 0.913931 | -0.0450087 | -0.000932610 | -0.000947947 |
| NOAA-6 | 0.908430 | -0.0354260 | -0.00646336 | -0.000142211 |
| NOAA-7 | 0.909891 | -0.0455624 | -0.000860797 | -0.00135342 |
| NOAA-8 | 0.908655 | -0.0405384 | -0.00342952 | -0.000783948 |
| NOAA-9 | 0.906832 | -0.0442841 | -0.00240122 | -0.00103459 |
| NOAA-10 | 0.908315 | -0.0349053 | -0.00947810 | 0.000947468 |
| NOAA-11 | 0.904380 | -0.0410871 | -0.00378272 | -0.000816891 |
| NOAA-12 | 0.913476 | -0.0449781 | -0.00101290 | -0.00127279 |
| NOAA-14 | 0.907108 | -0.0355551 | -0.00922134 | 0.000577326 |
| NOAA-15 | 0.903279 | -0.0413375 | -0.00664323 | 0.000255920 |
| NOAA-16 | 0.900686 | -0.0438801 | -0.00483903 | -0.000373348 |
| NOAA-17 | 0.904040 | -0.0399373 | -0.00761294 | 0.000343660 |
| NOAA-18 | 0.901034 | -0.0505245 | -0.00159713 | -0.000976422 |
| NOAA-19 | 0.903690 | -0.0334780 | -0.00707997 | 9.17525e-05 |
| Metop-A | 0.907438 | -0.0401103 | -0.00510746 | -0.000479942 |

**Table 6. Coefficients for the conversion of MODIS to AVHRR Channel-1 Reflectances for the DOME-C Target**

| Satellite | a | b | c | d |
|---|---|---|---|---|
| TIROS-N | 0.928385 | -0.00835046 | -0.00199140 | -8.49621e-05 |
| NOAA-6 | 1.00372 | -0.00105224 | -6.89875e-05 | -2.57574e-05 |
| NOAA-7 | 1.00749 | -0.000445622 | -4.25665e-05 | -1.21464e-05 |
| NOAA-8 | 1.00119 | -0.00173818 | -0.000875309 | -0.000352017 |
| NOAA-9 | 1.00092 | -0.00181081 | -0.00107680 | -0.000242925 |
| NOAA-10 | 1.01325 | -0.000402389 | -0.000815467 | -0.000353346 |
| NOAA-11 | 0.998424 | -0.00140001 | -0.000158452 | 4.65320e-05 |
| NOAA-12 | 1.00092 | -0.00181081 | -0.00107680 | -0.000242925 |
| NOAA-14 | 1.00562 | -0.00215960 | -0.000951781 | -0.000230314 |
| NOAA-15 | 1.01021 | -5.13580e-05 | -0.000191211 | -5.14452e-05 |
| NOAA-16 | 1.00846 | -0.000206034 | -6.25327e-05 | -2.19821e-05 |
| NOAA-17 | 1.01240 | 0.000100370 | 0.000142843 | 6.06139e-05 |
| NOAA-18 | 1.01254 | -9.08170e-05 | 0.000361382 | 0.000288593 |
| NOAA-19 | 1.00593 | 0.000121193 | -0.000249911 | -0.000212076 |
| Metop-A | 1.00728 | -0.000115979 | 0.000163312 | 9.38798e-05 |

**Table 7. Same as Table 4 except for Channel-2.**

| Satellite | a | b | c | d |
|---|---|---|---|---|
| TIROS-N | 0.918931 | -0.0315758 | -0.00545137 | 0.000151494 |
| NOAA-6 | 0.943126 | -0.0314111 | -0.00622665 | -0.000284891 |
| NOAA-7 | 0.929231 | -0.0329992 | -0.00629632 | -0.000107725 |
| NOAA-8 | 0.949067 | -0.0321892 | -0.00786617 | -0.000936539 |
| NOAA-9 | 0.940732 | -0.0344183 | -0.00813156 | -0.000679538 |
| NOAA-10 | 0.940876 | -0.0317480 | -0.00886553 | -0.00150398 |
| NOAA-11 | 0.941817 | -0.0330382 | -0.00663110 | -0.000252588 |
| NOAA-12 | 0.940732 | -0.0344183 | -0.00813156 | -0.000679538 |
| NOAA-14 | 0.922652 | -0.0333897 | -0.00744727 | -0.000690116 |
| NOAA-15 | 0.929517 | -0.0339015 | -0.00736506 | -0.000446061 |
| NOAA-16 | 0.918657 | -0.0348629 | -0.00610717 | 0.000103909 |
| NOAA-17 | 0.922661 | -0.0340303 | -0.00672706 | -0.000270731 |
| NOAA-18 | 0.903000 | -0.0361603 | -0.00519586 | 0.00119832 |
| NOAA-19 | 0.948005 | -0.0306886 | -0.00814826 | -0.00150935 |
| Metop-A | 0.924911 | -0.0332068 | -0.00595566 | 9.05989e-05 |

**Table 8. Final Calibration Slope Parameters for Channel-1 and Channel-2 for all AVHRR Sensors.**

| Satellite | Channel-1 | | | Channel-2 | | |
|---|---|---|---|---|---|---|
| | $S_0$ | $S_1$ | $S_2$ | $S_0$ | $S_1$ | $S_2$ |
| TIROS-N | 0.105 | 27.015 | -12.876 | 0.121 | 10.709 | -0.643 |
| NOAA-6 | 0.088 | 47.977 | -16.122 | 0.077 | 97.301 | -32.590 |
| NOAA-7 | 0.117 | 3.635 | 0.045 | 0.119 | 6.579 | -0.620 |
| NOAA-8 | 0.116 | 14.177 | -2.729 | 0.132 | 12.611 | -2.713 |
| NOAA-9 | 0.110 | 3.242 | 0.793 | 0.117 | 2.365 | 0.155 |
| NOAA-10 | 0.108 | 9.819 | -1.615 | 0.127 | 5.201 | -0.707 |
| NOAA-11 | 0.114 | 0.022 | 0.091 | 0.116 | 0.299 | 0.045 |
| NOAA-12 | 0.123 | 2.624 | -0.116 | 0.147 | 1.191 | -0.041 |
| NOAA-14 | 0.120 | 5.034 | -0.489 | 0.147 | 0.023 | 0.311 |
| NOAA-15 | 0.121 | 0.447 | -0.060 | 0.135 | 0.035 | 0.007 |
| NOAA-16 | 0.112 | 0.306 | 0.025 | 0.116 | 0.586 | 0.036 |
| NOAA-17 | 0.115 | 1.707 | -0.151 | 0.130 | 3.117 | -0.265 |
| NOAA-18 | 0.111 | 3.068 | -0.443 | 0.119 | 4.541 | -0.611 |
| NOAA-19 | 0.112 | -5.985 | -8.687 | 0.117 | 2.263 | 0.748 |
| Metop-A | 0.111 | 1.797 | -0.352 | 0.127 | 2.149 | -0.225 |

**Table 9. Calibration Slope Time Series Bias and Standard Deviation for Channel-1 and Channel-2. Statistics are percentages relative to the mean values.**

| Satellite | Channel-1 | | Channel-2 | |
|---|---|---|---|---|
| | Bias | Standard deviation | Bias | Standard deviation |
| TIROS-N | -0.096 | 2. 011 | 0.009 | 2.768 |
| NOAA-6 | -0.039 | 1.100 | 0.040 | 1.978 |
| NOAA-7 | 0.176 | 2.125 | -0.061 | 2.744 |
| NOAA-8 | 0.098 | 1.822 | -0.004 | 2.288 |
| NOAA-9 | -0.120 | 2.350 | -0.195 | 2.862 |
| NOAA-10 | 0.055 | 2.139 | 0.207 | 2.533 |
| NOAA-11 | -0.101 | 2.294 | 0.253 | 2.955 |
| NOAA-12 | -0.036 | 2.619 | 0.146 | 2.862 |
| NOAA-14 | -0.095 | 2.278 | 0.478 | 2.784 |
| NOAA-15 | -0.316 | 2.745 | 1.838 | 2.872 |
| NOAA-16 | -0.273 | 2.235 | 1.657 | 2.631 |
| NOAA-17 | -0.051 | 2.505 | 1.304 | 2.640 |
| NOAA-18 | -0.075 | 2.376 | 1.022 | 2.551 |
| NOAA-19 | -0.165 | 2.114 | 0.072 | 2.360 |
| Metop-A | -0.479 | 2.236 | 1.096 | 2.264 |

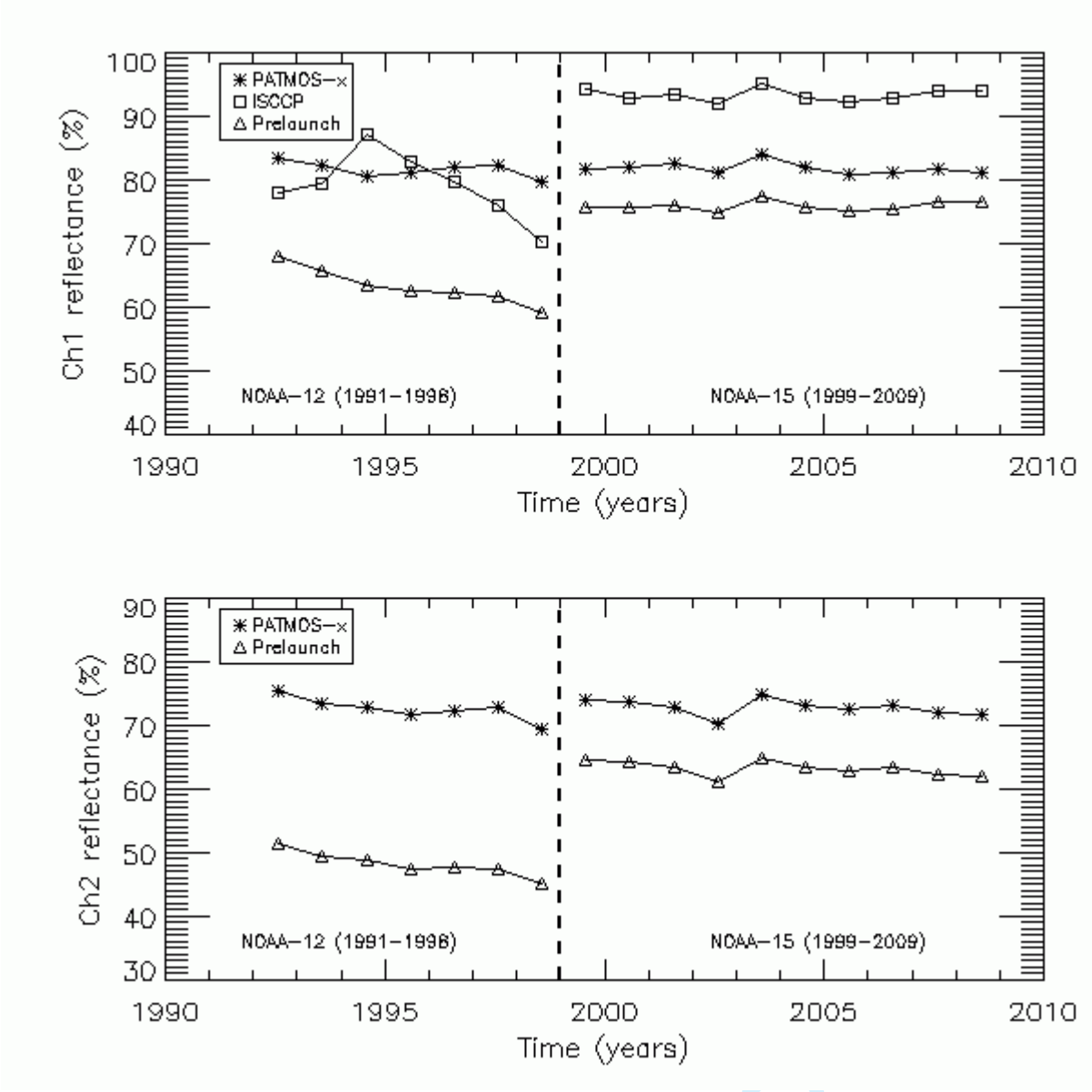


**Figure 1 Time-series of channel-1 (top) and channel-2 (bottom) reflectance over a target in Northern Greenland during July from 1992 to 2009. Target is defined by the region that spans from 73-78N and 32-48W. No filtering by solar or sensor geometry was performed. Values prior to 1999 are from NOAA-12 and values after 1999 are from NOAA-15. Vertical line designates transition from NOAA-12 to NOAA-15. There is no ISCCP channel-2 calibration.**

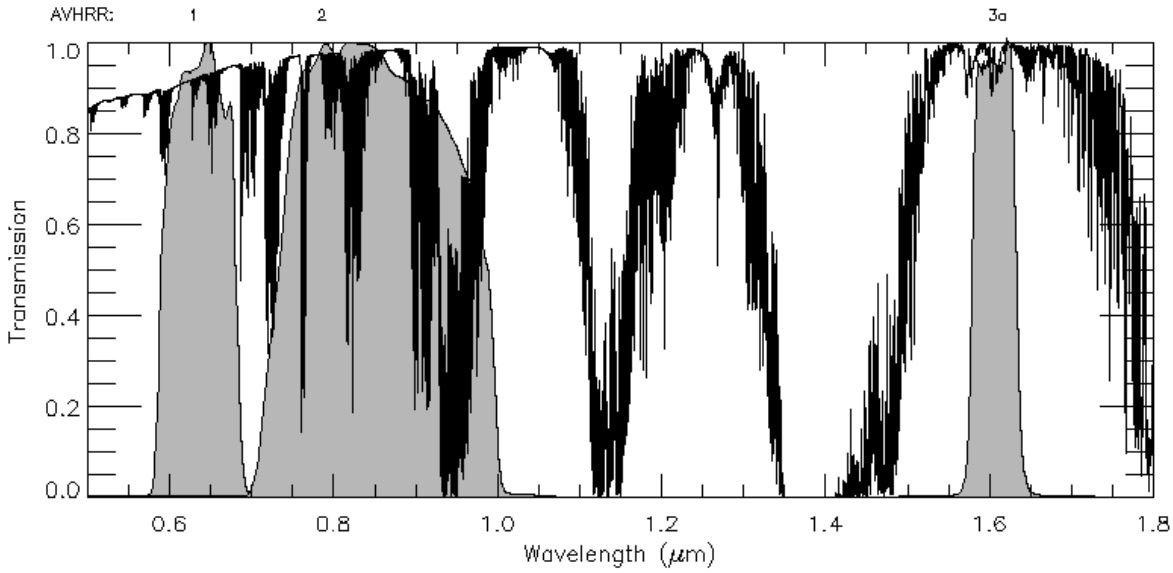


**Figure 2 NOAA-17 AVHRR solar reflectance channel spectral response functions (grey regions) overlaid onto a nadir transmission spectrum for a standard tropical atmosphere (McClatchey et al., 1971).**

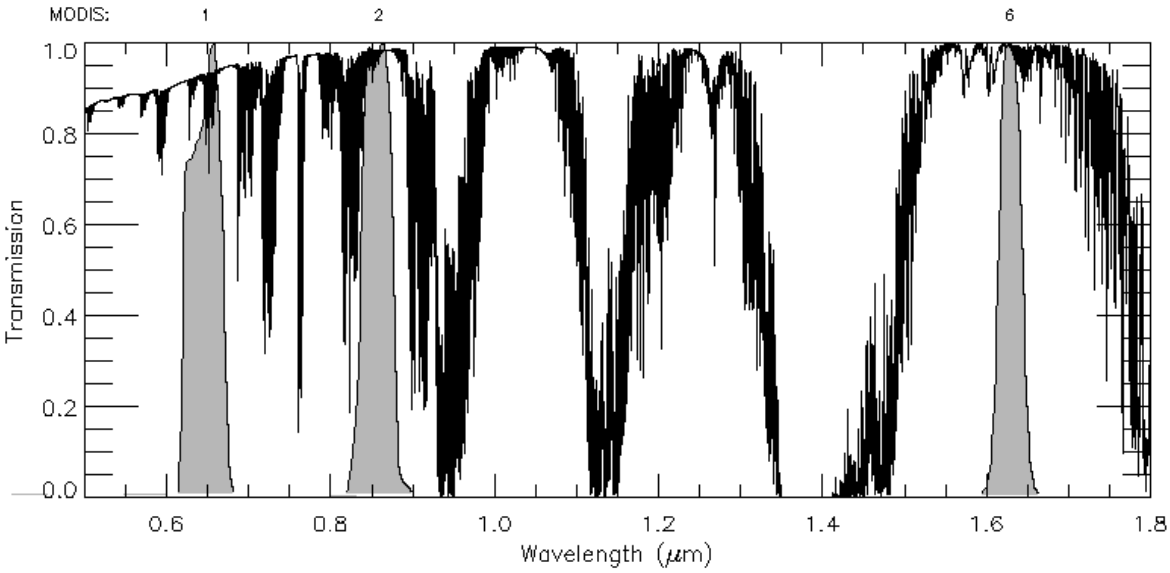


**Figure 3 Spectral response functions (grey-regions) of the TERRA/MODIS channels used to calibrate the AVHRR channel-1 and channel-2 overlaid onto a nadir transmission spectrum for a standard tropical atmosphere (McClatchey et al., 1971).**

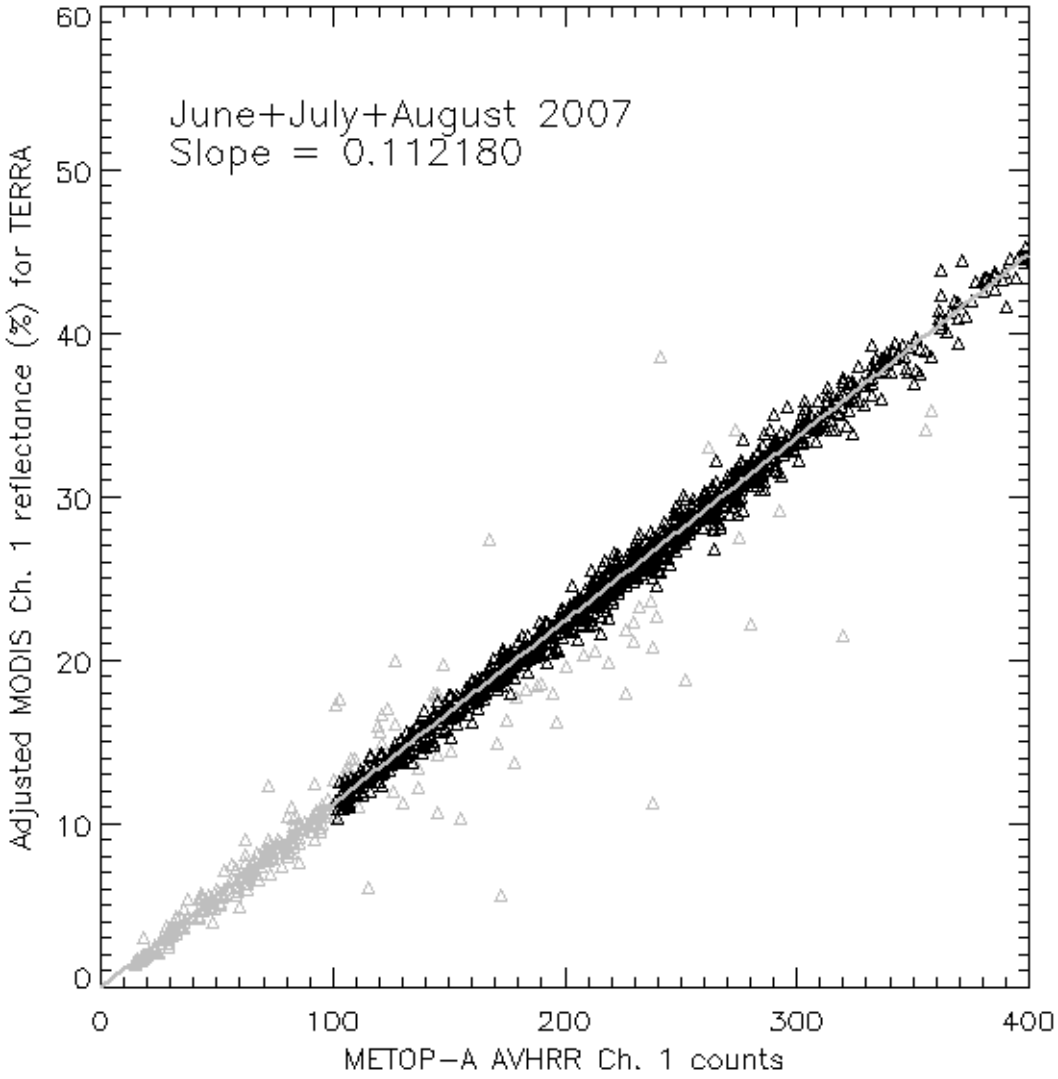


**Figure 4 Illustration of the SNO observations for 2007 summer season between one AVHRR sensor (METOP-A) and AQUA/MODIS. Grey points were excluded from the linear fit to estimate the calibration slope.**

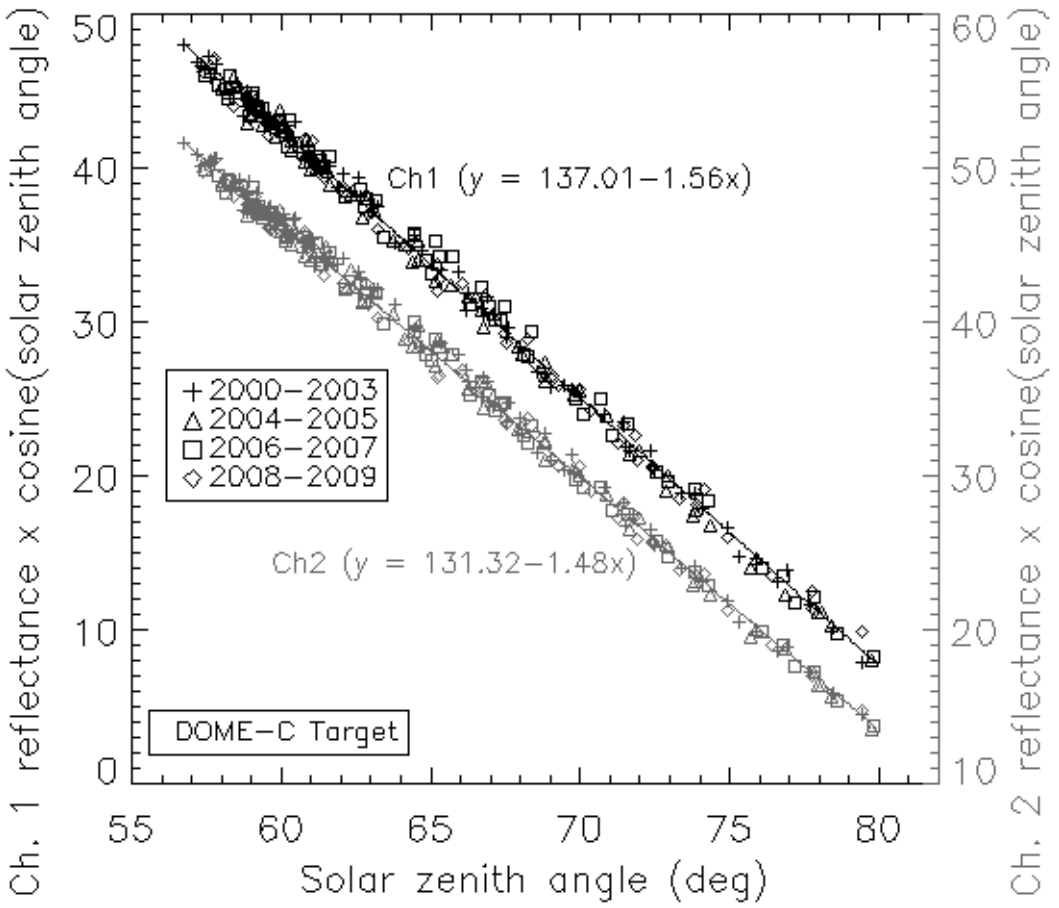


**Figure 5 Variation of the nadir MODIS channel-1 and channel-2 reflectance as a function of solar zenith angle over the DOME-C Target. Different symbols show values for different periods.**

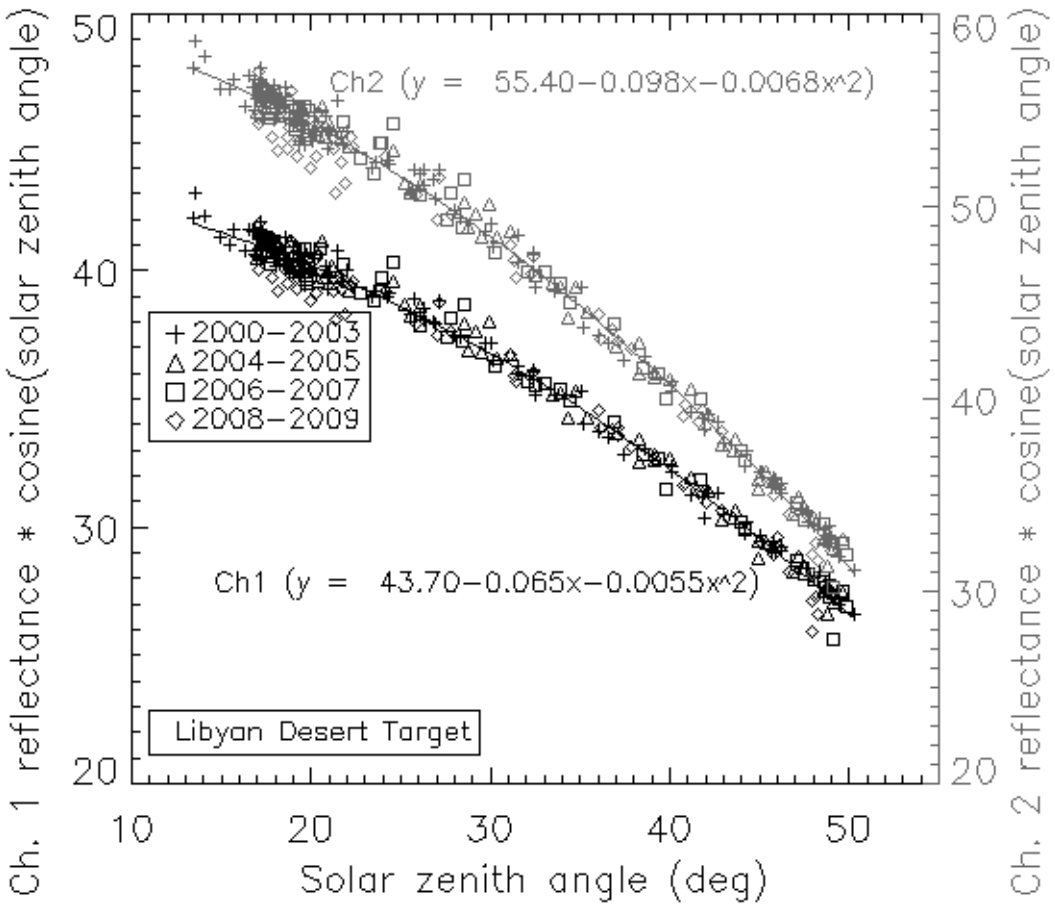


**Figure 6 Variation of the clear-sky nadir MODIS channel-1 and channel-2 reflectance as a function of the solar zenith angle for the Libyan Desert Target. Different symbols show values for different periods.**

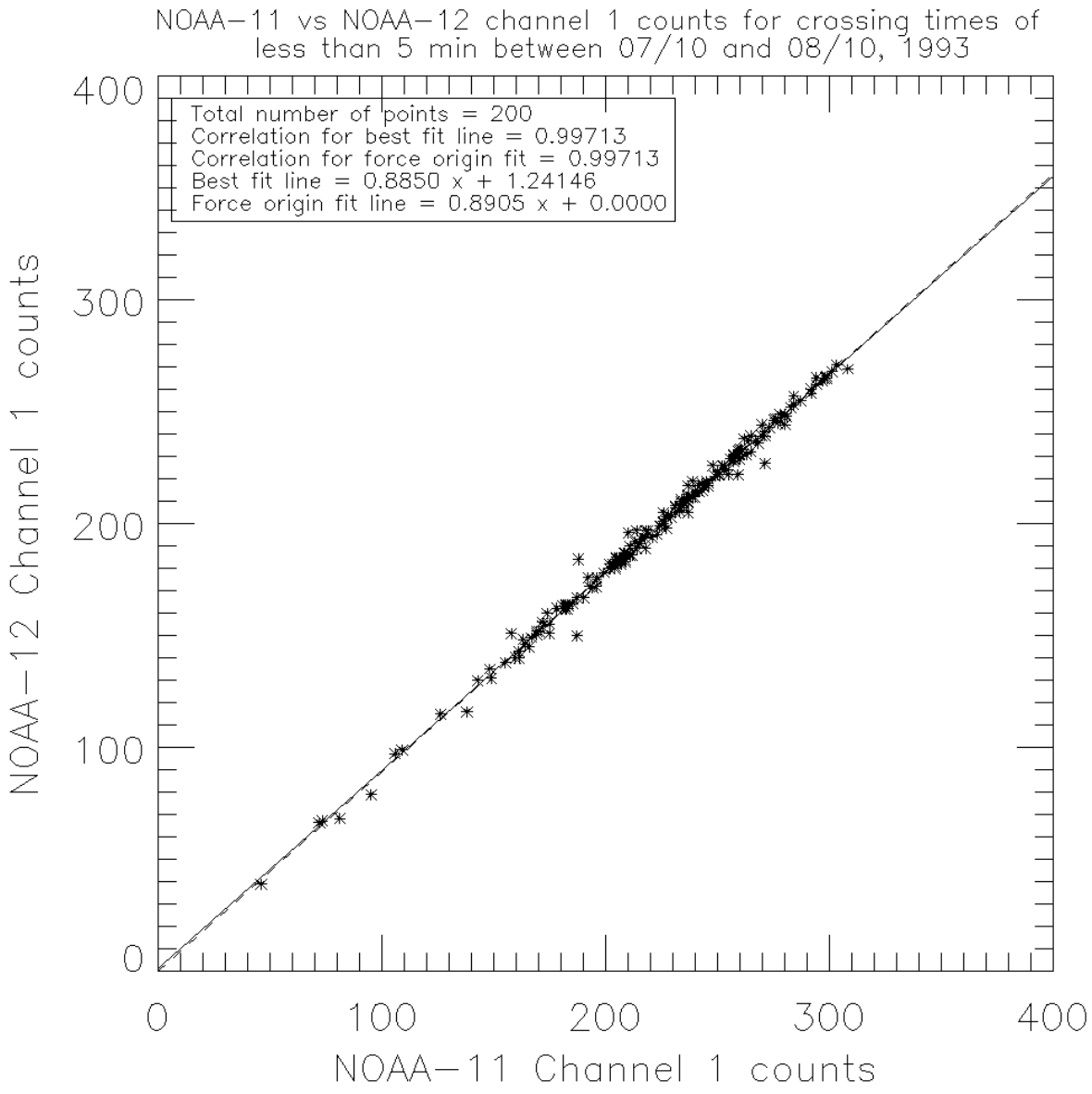


**Figure 7. Example of an AVHRR/AVHRR SNO.**

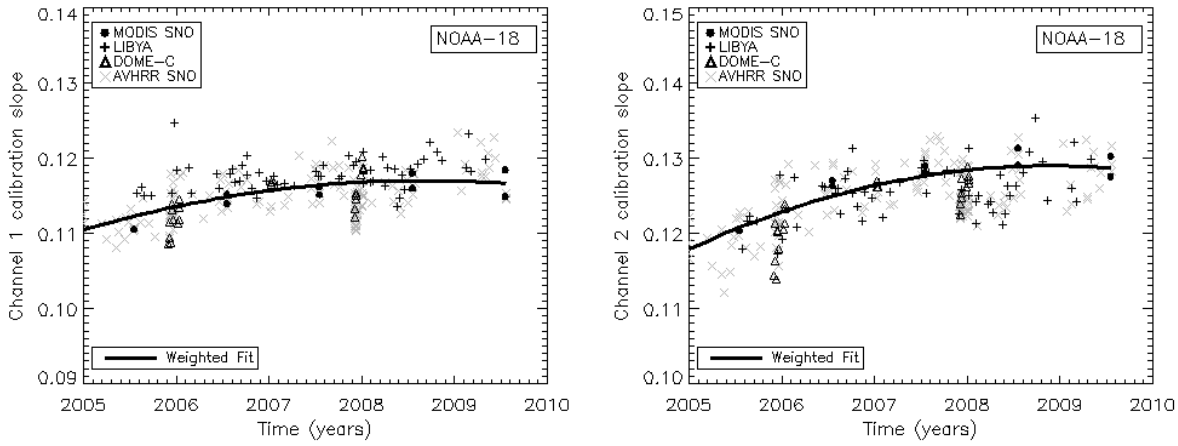


**Figure 8 Channel 1 and channel 2 calibration slope time series for NOAA-18. The solid line results from a weighted regression of the calibration slopes from the various methods. Table 8 and Table 9 provide the numerical regression coefficients and their statistics.**

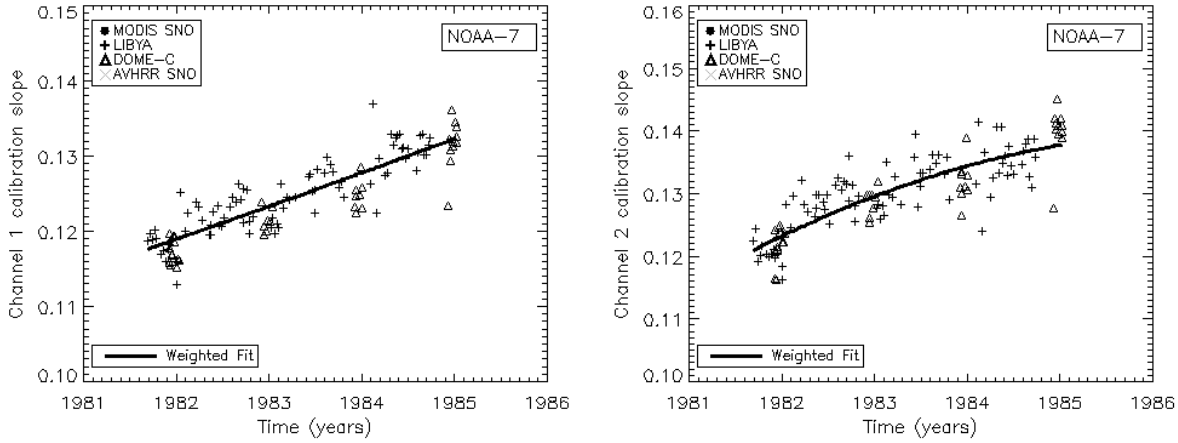


**Figure 9 Same as Figure 8 for NOAA-07.**

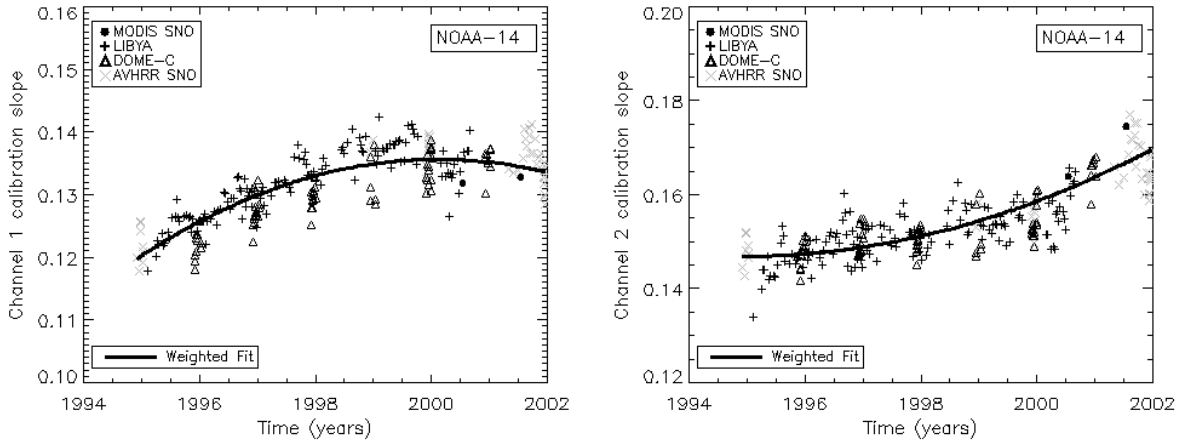


**Figure 10 Same as for NOAA-14.**

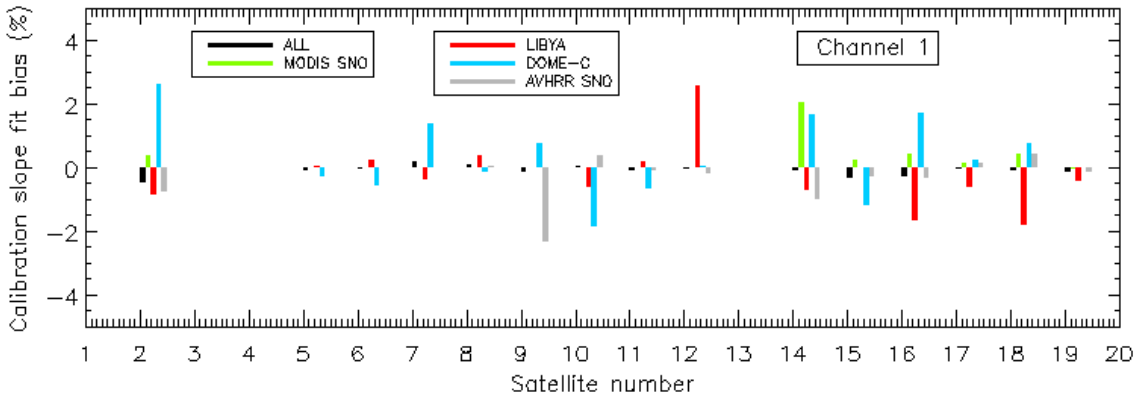


**Figure 11 Variation of channel-1 calibration slope biases with respect to the derived calibration slope for each satellite. Satellite number 2 is Metop-A and satellite number 5 is TIROS-N. Biases are computed as a percentage of the mean slope value over the life of the satellite. Values labeled "ALL" refer to the biases from all of the calibration sources.**

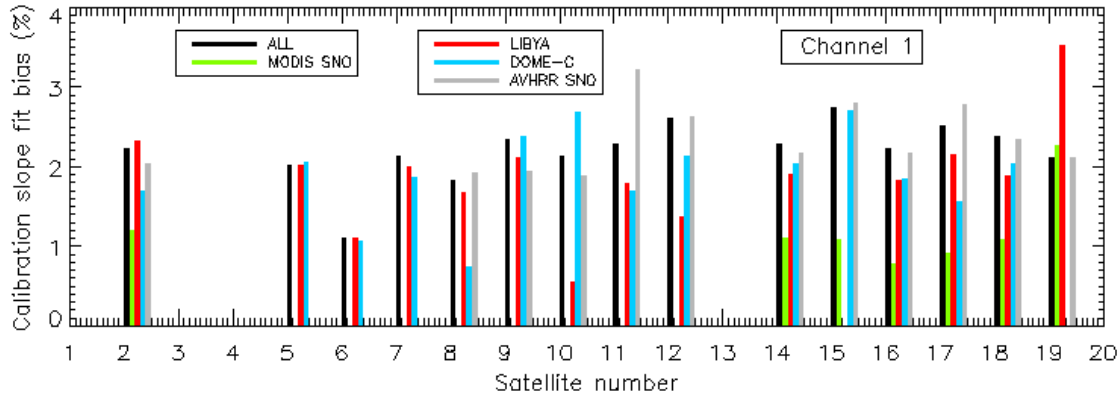


**Figure 12 Variation of the channel-1 calibration slope standard deviations with respect to the derived calibration slope for each satellite. Satellite number 2 is Metop-A and satellite number 5 is TIROS-N. Standard deviations are computed as a percentage of the mean slope value over the life of the satellite. Values labeled "ALL" refer to the standard deviations from all of the calibration sources.**

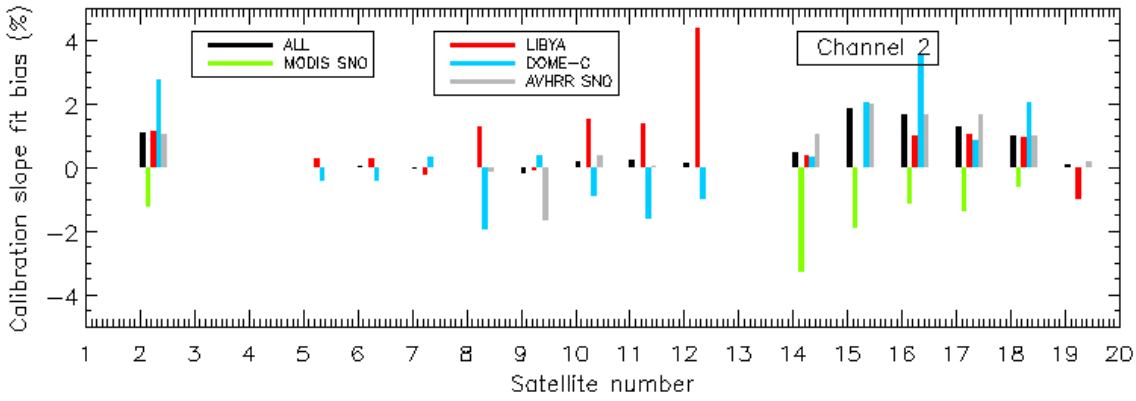


**Figure 13 Same as Figure 11 for channel-2.**

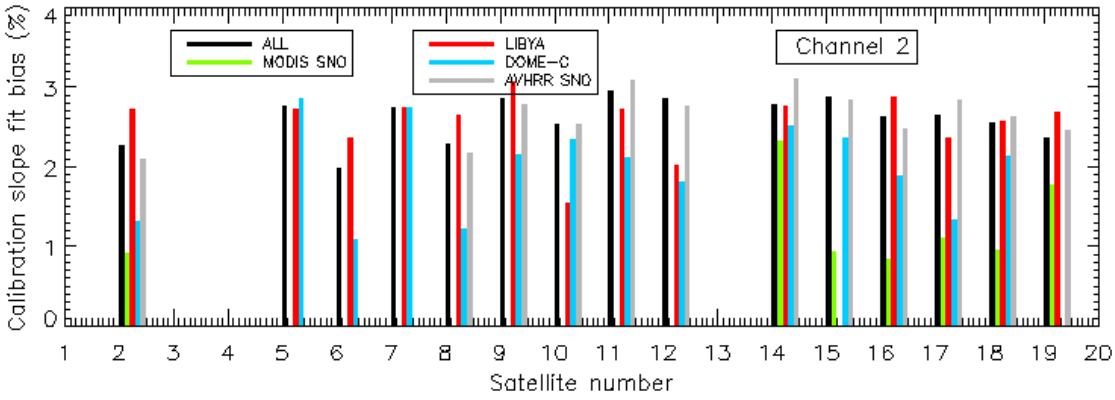


**Figure 14 Same as Figure 12 for channel-2.**